Holocene temperatures in southwestern Greenland controlled by topography, ice sheet proximity and oceanic conditions

Sudip Acharya[1,*], Allison A. Cluett[1,2], Amy L. Grogan[1], Jason P. Briner[1], Isla S. Castañeda[3], Elizabeth K. Thomas[1]

[1] Department of Earth Sciences, State University of New York at Buffalo, Buffalo, NY, USA
[2] University of California, Santa Cruz and NOAA Southwest Fisheries Science Center, CA, USA
[3] University of Massachusetts Amherst, Amherst, MA, USA

**Correspondence to*: Sudip Acharya (sudipach@buffalo.edu)

Abstract. The Holocene Thermal Maximum (HTM), a period during the Early and Middle Holocene when Greenland experienced a warmer climate than pre-industrial times, provides an ideal opportunity to test the sensitivity of the Greenland Ice Sheet to prolonged warmth. However, available climate reconstructions from the region provide a contrasting picture of the HTM—several reconstructions show an earlier HTM between the Early- to Middle-Holocene, while others show a delayed HTM between the Middle- to Late-Holocene. This discrepancy may be due to either the seasonal sensitivity of the proxies or to spatio-temporal climate variations. Here we generate five new Holocene timeseries of branched glycerol dialkyl glycerol tetraether (brGDGT)-inferred mean air temperature for months above freezing from lakes along a latitudinal transect in southwestern Greenland, yielding a total of seven Holocene brGDGTs-inferred timeseries in this region. Decoupled Holocene trends between the ratio caldarchaeol to crenarchaeal and methylation of branched tetraethers index (MBT'_{5Me}) and the isomer ratio of 5- to 6-methyl brGDGTs (IR_{6Me}) in individual lakes suggest brGDGTs in these lakes are primarily influenced by temperature. Lake model sensitivity tests suggest minimal intra-lake variation in both the seasonal production window of brGDGTs and the sensitivity of studied lakes to air temperature changes, suggesting regional climate as a primary mechanism influencing these timeseries. Five of the brGDGT timeseries suggest a temperature maximum between approx. 7 and 5 ka, following peak summer insolation and in agreement with many regional reconstructions. A coastal site experienced a temperature maximum between approx. 5 to 3 ka, coinciding with nearby sea surface temperature reconstructions, suggesting this site is influenced strongly by ocean-atmosphere heat exchange. A site far from both the coast and the Greenland Ice Sheet suggests peak warmth in the Early Holocene. These results based on a single proxy suggest that southwestern Greenland largely experienced similar Holocene summer temperature trends, but some local temperature variations occurred due to proximity to the ice sheet and ocean. Further investigations quantifying seasonal sensitivity between proxies and local effects (e.g., site-specific systematics, and proximity to ice sheet and ocean) may reveal more similarities among proxy timeseries than previously reconstructed.

1 Introduction

Arctic warming has profound and far-reaching impacts on the region's environment (Rantanen et al., 2022; Thoman et al., 2023). For example, the Greenland Ice Sheet has been melting at an increasing rate, causing sea level rise (Dutton et al., 2015; Frederikse et al., 2020). Ocean circulation and biogeochemical cycles have also undergone significant changes (Vihma et al., 2016; Wrona et al., 2016). Nutrient input into lakes have increased due to permafrost thawing (Reyes and Lougheed, 2015), leading to summer stratification and enhanced microbial respiration (Antoniades et al., 2024; Jane et al., 2023; Klanten et al., 2023; Prowse et al., 2011). These changes raise serious concerns about the future of the Arctic environment as global warming continues. However, available climate model projections show inter-model differences (IPCC, 2021; Seneviratne and Hauser, 2020), making it difficult to accurately predict the future. To improve our understanding of the sensitivity of the Arctic system, glaciers, and the water cycle to future climate changes and to improve climate model capability, a long-term perspective on past climate changes and causal mechanisms is required (Axford et al., 2021; Briner et al., 2016).

The Holocene epoch (11.7 thousand years before present [ka] to 0 ka) on Greenland is characterized by millennia of relatively warm climate during the Early to Middle Holocene, likely warmer than preindustrial, and subsequent gradual cooling until 1850 CE, generally tracking boreal summer insolation (Axford et al., 2021; Briner et al., 2016; Kaufman et al., 2020). During the Early and Middle Holocene, the region around Greenland experienced major environmental changes: mountain glaciers were either smaller or entirely absent (Larocca et al., 2020; Larocca and Axford, 2022; Larsen et al., 2017; Schweinsberg et al., 2017, 2019), and the Greenland Ice Sheet was smaller compared to its current extent (Briner et al., 2020; Larsen et al., 2015; Leger et al., 2024), potentially causing changes in atmospheric circulation (Masson-Delmotte et al., 2005; Thomas et al., 2016, 2023). However, the patterns of Holocene climate change in Greenland are still poorly resolved. This is in part due to site-specific, proxy-to-proxy, and proxy-model disagreement (Axford et al., 2021; Briner et al., 2016; Liu et al., 2014; Martin et al., 2024). Therefore, quantifying temperature variations throughout Greenland during this epoch is of particular interest.

The Southwestern Greenland Ice Sheet (defined herein as the region from Nuussuaq to Cape Farewell, Figure 1) is highly sensitive to Holocene climate and environmental perturbations, due to its proximity to Atlantic Ocean deepwater formation, with attendant variability in heat and moisture transport (Downs et al., 2020; Lazier et al., 2002; Lesnek et al., 2020; Yang et al., 2016; Young et al., 2020). Holocene temperature timeseries from the ice-free areas in this region are mainly derived from lacustrine proxies, including pollen, chironomids, and biomarkers (Axford et al., 2021; Briner et al., 2016; Gajewski, 2015; Kaufman, 2004). Although most of the existing time series show gradual cooling throughout the Late Holocene, they disagree on the timing and magnitude of the temperature maximum, with evidence for an earlier and larger temperature maximum farther north, but with differences between archives and proxies (Axford et al., 2021; Briner et al., 2016; Gajewski, 2015; Kaufman, 2004; Larocca and Axford, 2022).

Reconstructions of Greenland Ice Sheet margin positions between Ilulissat and Kangerlussuaq suggest rapid retreat and warmest summers between ~10.4 and 9.1 ka (Lesnek et al., 2020), a time period not covered by many other terrestrial archives. An annual temperature reconstruction based on argon and nitrogen isotopes from the Greenland Ice Sheet Project (GISP2) ice core reveals a Holocene thermal maximum (HTM) at ~7.9 to 6 ka, or 10 to 7.5 ka when considering possible elevation changes with temperature ~3 to 5 °C warmer than the recent decades (Axford et al., 2021; Kobashi et al., 2017) (Fig. 1; point 6). Chironomid-inferred July air temperatures from North Lake near Ilulissat (Fig. 1, point 10) shows the warmest period of the past 7 ka between ~6 and 4 ka, with temperatures ~2 to 3 °C higher than preindustrial (Axford et al., 2013). A branched glycerol dialkyl glycerol tetraether (brGDGT)-inferred summer lake water temperature time series from Lake Gus between Kangerlussuaq and Sisimiut reveals maximum temperature of the past 9 ka from 9 to 6 ka (Cluett et al., 2023) (Fig. 1, point 11), whereas brGDGTs from Lake 578 in southern Greenland reveals the warmest period in the past 11 ka from ~7.5 to 4.5 ka, with ice-free season temperature ~4 to 6 °C higher than preindustrial in both timeseries (Schneider et al., 2024) (Fig. 1, point 14). Alpine glaciers from southern Greenland were at their smallest extent between ~7.3-7.1 ka, implying warmest temperature in the past ~10.5 ka, with air temperature only ~1 to 2 °C above present (Larocca et al., 2020) (Fig. 1; point 15, 18). Pollen based reconstructions from Lake Qipisarqo suggest that the thermal maximum of the past 8.5 ka occurred between ~7 and 5 ka, with summer air temperatures up to ~5 °C higher than pre-industrial (Frechette and de Vernal, 2009) (Fig. 1; point 12). In contrast, nearby pollen-based reconstructions from Spongilla Sø and Comarum Sø imply warmest summers of the past 10.5 ka occurred after 5.2 ka, with temperatures ~1 to 2 °C higher than present (Fredskild, 1973; Gajewski, 2015) (Fig. 1; point 14 and 16). Additionally, marine reconstructions indicate the HTM between ~6 and 2 ka, with summer sea surface temperatures (SST) up to ~5 °C higher than present (Axford et al., 2021; Hansen et al., 2020; Ouellet-Bernier et al., 2014).

Several mechanisms have been called upon to explain the different timing and magnitude of peak warmth: differing seasonal sensitivity of proxies, ice sheet meltwater influence causing delayed warmth in marine archives, and vegetation lags causing delays in pollen records (Axford et al., 2021; Briner et al., 2016). Some of these mechanisms can be tested by generating time series from the same proxy in similar archives along a spatial gradient, thus avoiding possible differences caused by the archive/proxy.

Here we developed new timeseries of brGDGT-inferred mean air temperatures for months above freezing (MAF) from five lakes along a latitudinal transect from 64 to 69° N (Fig. 1) in southwestern Greenland, spanning the past 9 ka. BrGDGTs are membrane-spanning lipids of bacteria (Sinninghe Damsté et al., 2000) and they are well preserved in lake sediments (Castañeda and Schouten, 2011; Schouten et al., 2013). BrGDGTs distributions are primarily influenced by temperature (Raberg et al., 2021) and therefore this proxy has shown promise as a quantitative high-latitude terrestrial paleotemperature proxy (e.g., Cluett et al., 2023; Lindberg et al., 2022; Schneider et al., 2024; Thomas et al., 2018). However, the influence of site-specific factors such as sub-oxic conditions (van Bree et al., 2020; Raberg et al., 2025; Weber et al., 2018; Wu et al., 2021), lake ice cover duration (Shanahan et al., 2013), and microbial ecology (Liang et al., 2024) should also be taken into consideration before reconstructing temperature. To investigate the influence of site-specific variations such as mixing regimes that may cause sub-oxic conditions, duration of ice cover, and differing sensitivity of each lake to air temperature change, we ran the lake energy, hydrologic, and isotopic mass balance model developed by (Dee et al., 2018; Hostetler and Bartlein, 1990) and updated by (Morrill et al., 2019) for each lake under modern and perturbed climate scenarios. Overall, we aim to investigate (1) Holocene temperature evolution in southwestern Greenland, and (2) Possible causes of temporal differences in temperature maxima.

2 Materials and methods

2.1 Study area and coring

We studied five lakes in southwestern Greenland with informal names: Pluto, N3, Rosaea, Marshall, and Bullet (Fig. 1). None of the lakes currently receive ice-sheet meltwater. Table 1 has detailed geographical and morphological features of each lake. Lakes Pluto (69.109° N, 51.032° W, 190 m asl; Fig. 1; point 1) and N3 (68.636° N, 50.981° W, 59 m asl; Fig. 1; point 2) are situated south of Ilulissat, western Greenland. Watershed vegetation consists of dwarf shrub heath, dominated by *Salix* sp. and *Betula* sp. (Bennike, 2000). On July 27, 2010, during core collection, depth profiles of temperature, conductivity, salinity, pH and dissolved oxygen were measured in Lake N3 (Corcoran et al., 2021; Thomas et al., 2016). During the field expedition in July 2009 (Pluto Lake) and late July 2010 (N3), both lakes had small inflowing streams and active channelized outflows. For more details see Thomas et al., (2016; 2020).

Table 1: Geographical and morphological characteristics including site ID in Fig. 1, latitude (lat), longitude (lon), elevation (m asl), catchment area (km^2), maximum depth (m), surface area (km^2), and closest estimated distances from Ice Sheet and Ocean (km^2) of study lakes (Pluto, N3, Rosaea, Marshall, and Bullet), Lake Gus (Cluett et al., 2023) and Lake 578 (Schneider et al., 2024).

Site ID. in Fig 1.	Lake name	Lat (°)	Lon (°)	Elevation (m asl)	Catchment area (km^2)	Maximum depth (m)	Surface area (km^2)	Distance from modern ice sheet (km)	Distance from ocean (km)
1	Pluto	69.109	-51.032	190	1.21	4	0.07	36	2
2	N3	68.636	-50.981	59	0.72	16	0.09	14	2
11	Gus	67.032	-52.427	300	4.61	6	0.09	100	65
3	Rosaea	66.982	-53.718	228	1.03	9	0.01	160	3
4	Marshall	64.464	-49.431	862	0.56	8	0.02	<0.5	150
5	Bullet	63.982	-49.537	944	0.30	8	0.02	1.5	100
13	578	61.080	-45.609	155	0.82	16	0.06	35	76

Lake Rosaea (66.982° N, 53.718° W; Fig. 1; point 3) is situated approx. 5 km north of Sisimiut on western Greenland and 3 km from the coastline with Davis Strait. Watershed vegetation consists of shrubs including *S. glauca* and *S. herbacea* on hill slopes while *Empetrum nigrum*, *Betula nana*, and *Rhododendron tomentosum* are present on low-lying ground. Patches of snowpack were observed around the lake and at the higher elevations during the field expedition on July 18–21, 2018. Also, during that summer, the lake was fed by multiple active channelized inflow streams, and it had an outflow stream.

Marshall (64.464° N, 49.431° W, 862 m asl; Fig. 1; point 4) and Bullet (63.982° N, 49.537° W, 944 m asl; Fig. 1; point 5) lakes are situated inland of Nuuk in southwestern Greenland. Marshall Lake is <2 km outboard of the modern ice sheet margin and received ice-sheet meltwater briefly during the historical maximum extent. Bullet Lake is located approx. 60 km south from Marshall Lake. Lake catchment consists of vegetation including *Vaccinium uliginosum*, *E. nigrum*, *S. herbacea*, and *Sphagnum* sp. Both Marshall and Bullet lakes catchments include shrubs and grasses on hillslopes and *Eriophorum scheuchzeri,* and *Sphagnum* sp. around the shoreline. Both Marshall and Bullet lakes do not have channelized inflow and outflow streams.

The climate in coastal southwestern Greenland is influenced by atmospheric and oceanic conditions (Box et al., 2023; Westergaard-Nielsen et al., 2020). In the summer, moisture from North America contributes to the region, while in the winter, evaporation from proximal seas becomes the dominant moisture source (Cluett et al., 2021; Nusbaumer et al., 2019). Precipitation is relatively high in the southernmost part of the coast and decreases with increasing latitude (Cluett et al., 2021). From June to September, temperature is above freezing, while during the winter months, it drops well below freezing. Temperature generally decline northward along the coast and with increasing elevation, where snow cover and radiative cooling are more pronounced (Karami et al., 2017). The West Greenland coastal current carries warm water from the North Atlantic Ocean to Baffin Bay, and influences climate in coastal southwestern Greenland (Westergaard-Nielsen et al., 2020), whereas the southernmost land on western Greenland is influenced by the east Greenland current, which carries cold Arctic water around the southern tip of the island.

2.2 Sediment core chronology

^{14}C-ages and age-depth models for the sediment cores from lakes N3 and Pluto are published by Thomas et al. (2016) and Thomas et al. (2020). Here, we updated the age-depth models for the lakes employing the IntCal20 calibration curve (Fig. S1–2). Additionally, we developed age-depth models for Marshall, Bullet and Rosaea lakes (Fig. S3–5). The age-depth model for Marshall Lake is derived from ^{14}C ages from seven aquatic moss macrofossils, Bullet and Rosaea Lakes derived from nine aquatic macrofossils (Tables S1–S3). All the age-depth models were calculated using rbacon within the GeoChronR package using IntCal20 (Blaauw and Christen, 2011; McKay et al., 2021).

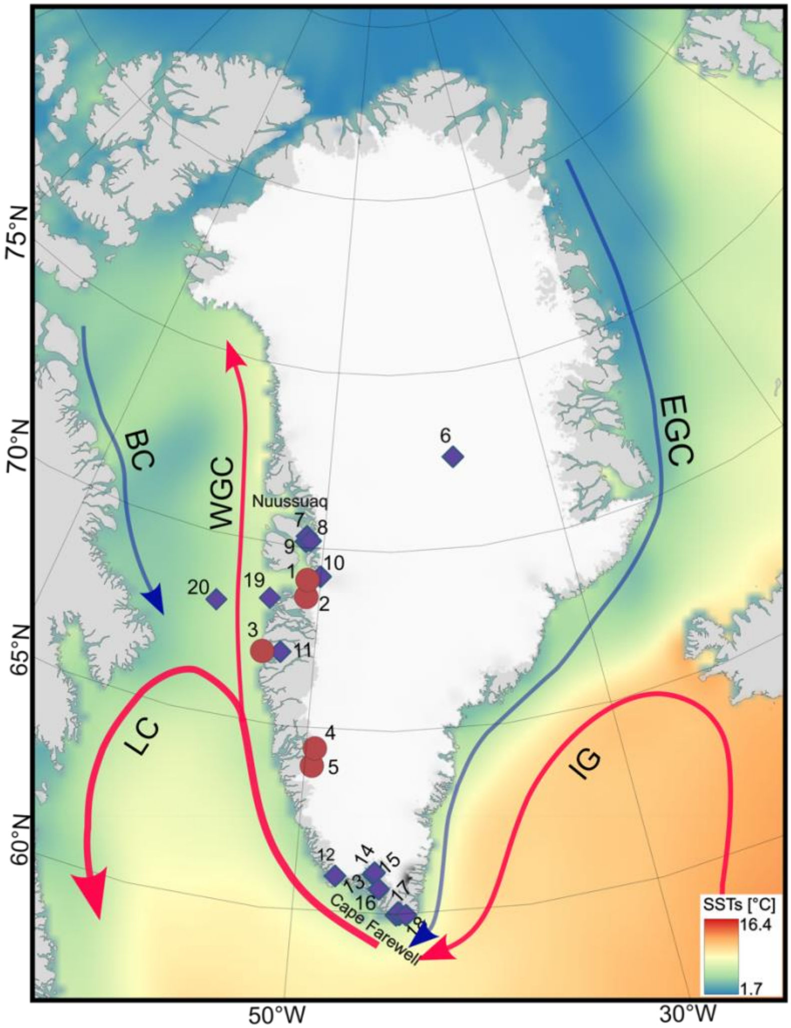

Figure 1: Map of Greenland and surrounding area showing study lakes in red circles (1–5), sites mentioned in the text in blue diamonds (6–20) and ocean currents; WGC: West Greenland, EGC: East Greenland, IG: Irminger, BC: Baffin, and LC: Labrador currents. Site numbered as follows: (1) Pluto, (2) N3, (3) Rosaea, (4) Marshall (5) Bullet (6) GISP2 (Kobashi et al., 2017), (7) Sermikassak, (8) Qangattaq ice cap (9) Saqqap Tasersua (Schweinsberg et al., 2017, 2019) (10) North Lake (Axford et al., 2013) (11) Lake Gus (Cluett et al., 2023) (12) Qipisarqo (Frechette and de Vernal, 2009; Kaplan et al., 2002) (13) Lake 578 (Schneider et al., 2024) (14) Spongilla Sø (Fredskild, 1973; Gajewski, 2015) (15) Alakariqssoq glaciers (Larocca et al., 2020) (16) Comarum Sø (Fredskild, 1973; Gajewski, 2015) (17) N14 (Andresen et al., 2004), (18) Quvnerit glaciers (Larocca et al., 2020), and marine sediment cores (19) MSM343300 (Ouellet-Bernier et al., 2014) and (20) CC70 (Gibb et al., 2015). The fill colour represents modern summer sea surface temperatures (SSTs) (Fisher et al., 2023; Moon et al., 2023).

2.3 Biomarker analysis

We used the method described in Cluett et al. (2023) for the extraction and purification of GDGTs. Briefly, total lipids from homogenized 0.5 to 2 g of bulk sediment samples were extracted using a Dionex Accelerated Solvent Extractor 200 with 30 ml of dichloromethane (DCM): methanol 9:1 (volume:volume, v:v). Afterwards, 0.1 µg of a C_{46} glycerol dialkyl glycerol tetraether (GDGT) was added to the total lipid extracts (TLE). TLEs were separated into neutral and acid fractions using aminopropyl silica gel columns eluted with DCM:isopropanol (2:1 v:v) and acids with 4% acetic acid in DCM, respectively. Neutral fractions were further split into apolar, ketone, and polar fractions using alumina columns eluted with hexane:DCM (9:1, v:v), hexane:DCM (1:1, v:v), and DCM:MeOH (1:1, v:v), respectively. GDGTs contained in the polar fraction were filtered using 0.45 µm PTFE filters. GDGTs were analyzed on an Agilent 1260 Ultra High-Performance Liquid Chromatograph (UHPLC, Agilent 1260) coupled to an Agilent 6120 Mass Selective Detector (MSD) in selected ion monitoring (SIM) mode in the Biogeochemistry Laboratory at the University of Massachusetts Amherst. For the separation of 5-methyl and 6-methyl isomers, we used two coupled waters UHPLC columns (150 mm * 2.1mm*1.7 µm) and followed the procedure described by Hopmans et al. (2016). Chromatography was performed applying a three-phase isocratic solvent gradient using 100% hexane (solvent A) and hexane:isopropanol (9:1, v:v, solvent B). Peak integration was done using the "chromatoPy" package in Python (Otiniano et al., 2025). We determined the GDGT concentrations in relation to the C_{46} internal standard.

We analyzed 23 samples from Pluto Lake at ~4 cm resolution, 69 samples from Lake N3 at ~3 cm resolution, 44 samples from Rosaea Lake at ~6 cm resolution, 23 samples from Marshall Lake at ~4 cm resolution, and 22 samples from Bullet Lake at ~7 cm resolution. All samples were from 0.5-cm-thick subsamples of sediment cores. The GDGT time series from Lake N3 is at 100-year-resolution for the past 8 ka. Those from lakes Pluto, Marshall, and Bullet provide 400-year-resolution, covering from 9 to 2 ka, 9 to 1 ka, and 9 to 1 ka, respectively. The GDGT time series from Lake Rosaea offers a 200-year-resolution, spanning from 9 to 1 ka.

2.4 Lake modelling

We ran sensitivity tests of the lake energy and water balance model developed by (Dee et al., 2018; Hostetler and Bartlein, 1990) and modified by (Morrill et al., 2019). We used ERA5 climate data (air temperature, relative humidity, wind speed, incoming surface shortwave radiation, downward longwave radiation, surface pressure, and precipitation amount) averaged over the four grid boxes nearest each lake for January 1, 1994, to December 31, 2024, as meteorological input data (Muñoz Sabater, 2019). All the meteorological inputs were at a 6-hourly timestep except total precipitation amount, which is hourly timesteps summed to total 6-hourly precipitation amount. Lake surface areas were estimated using Google Earth, and catchment areas using Arctic DEM in QGIS (Porter et al., 2022). Depth-area slices at a resolution of 1 meter were estimated using bathymetry of each lake (Zhao et al., 2021), which was determined either using sonar or by depth sounding with a weighted measuring tape. We ran the lake model for 30 years, with a 10-year spin-up period at the beginning using 1994 meteorological input data. For lakes Bullet, Marshall, Pluto, Rosaea, and 578, we used the model parameters as for Lake Gus

(Cluett et al., 2023), as these lakes have similar depths and comparable surface areas. For Lake N3, we used the lake model parameters defined by Corcoran et al., (2021) for the lake. We acknowledge that using the same lake model parameters might lead to data-model mismatches with lake conditions, however for the purpose of sensitivity tests on orbital scales, such changes can only have a minor impact (Fig. S17–S19). To evaluate the sensitivity of lakes to changes in air temperature we perturbed the ERA5 input annual, and summer (defined as June to September) temperature by ±10, ±6, ±4, and ±2 °C. To evaluate the impact of shading on the lake water temperature, we perturbed the incoming short-wave radiation by ±10, ±25, and +50%. We calculated shading by surrounding topography on for each lake using GDAL in python using Arctic DEM for daytime (sunset to sunrise) at 15-minute time steps every 10 days from April to September under modern insolation parameters. Wind direction at each lake was calculated using 6-hourly ERA5 climate data from January 1, 1994, to December 31, 2024.

3. Results and discussion

3.1 Anoxia, sources of brGDGTs and temperature implications

Total brGDGT concentration in these lake sediments from southwestern Greenland was about 6 to 10 times higher than total isoprenoid GDGT (isoGDGT), with both revealing a similar downcore pattern in all lakes, peaking in the early Holocene and declining towards the Late Holocene (Fig. S6–S10). Caldarchaeol (GDGT-0) is the most abundant isoGDGT (Fig. S11a), followed by crenarchaeol (GDGT-4) and GDGT-1, whereas GDGT-2, GDGT-3, and the crenarchaeol isomer (GDGT-4′) were below detection limit in many samples, restricting TEX_{86}-based temperature reconstruction (Schouten et al., 2002). Caldarchaeol is produced in anaerobic conditions in lake water or sediments by methanogenic *Euryarcheota* or heterotrophic *Bathyarchaea* (Buckles et al., 2013; Sinninghe Damsté et al., 2009), whereas crenarchaeol is produced in aerobic lake water and sediments by *Thaumarchaeota* (Baxter et al., 2021; Besseling et al., 2018). The activity of anaerobic archaeal communities is higher during winter in ice-covered lakes (Baxter et al., 2021; Blaga et al., 2011; Butler et al., 2019; Massé et al., 2019; Sinninghe Damsté et al., 2009). Therefore the ratio of caldarchaeol to crenarchaeol (Cald/Cren) may be a sensitive indicator of winter suboxic conditions in the water column and/or lake sediments, where the caldarchaeol is produced (Blaga et al., 2009). Cald/Cren ranged from 1 to 857 in all study lakes, with generally low values in lakes Marshall and Rosaea and high values in lakes Bullet, N3 and Pluto (Fig. 2a). Cald/Cren was higher from 10 to 6 ka in lakes Pluto, Rosaea, Bullet, and Marshall, which may indicate lower oxygen availability (Acharya et al., 2023; Baxter et al., 2021; Blaga et al., 2009) (Fig. 2a). After approx. 6 ka, the Cald/Cren remained relatively low and stable, indicating oxic lake sediments and/or water column. Cald/Cren in Lake N3 had higher values indicating suboxic conditions from 7.5 to 5 ka, and lags the decrease recorded in other lakes by about a millennium (Fig. 2a). We hypothesize that this could be related to a greater maximum depth (~17 m) of N3 compared to other lakes (<10 m water depth). Deeper conditions favor greater stratification, which could prolong suboxic conditions (Kerimoglu and Rinke, 2013). This Early Holocene timing of high Cald/Cren is similar to results from other Arctic lakes (Cluett et al., 2023; McFarlin et al., 2023; Schneider et al., 2024) and is probably caused by prolonged thermal stratification due to longer ice cover duration and/or summer warming due to high summer insolation (Klanten et al., 2023; MacIntyre et al., 2018).

BrGDGTs in lake sediments can be allochthonous – produced in the catchment soil and transported to the lake via runoff erosion, and autochthonous – produced in the water column and surface sediment (Baxter et al., 2021; Tierney et al., 2012). BrGDGTs produced in these diverse environments can have different responses to environmental conditions, directly impacting the temperature reconstruction (Acharya et al., 2023; Martin et al., 2020). Therefore, understanding the sources of brGDGTs is crucial before temperature reconstruction. We evaluated the sources of brGDGTs in southwestern Greenland lakes by comparing their distributions with those from high latitude (>50 °N) soil, peat, and lake sediment samples (Raberg et al., 2022). BrGDGTs from southwestern Greenland lakes have different fractional abundance of hexa-, penta- and tetra-methylated brGDGTs than those in peat and soil samples but are similar to high-latitude lake surface sediment samples (Fig. S11), suggesting lacustrine origin. Furthermore, brGDGT IIIa, which is produced in higher relative abundance in lake water than in soils (Weber et al., 2018), is abundant in the southwestern Greenland lake sediments, similar to high-latitude lake surface sediments, and greater than in high-latitude soils (Fig. S11). This corroborates the autochthonous production of brGDGTs in southwestern Greenland lakes, although there remains a possibility of minor brGDGT contributions from the surrounding catchment.

Air temperature in southwestern Greenland is above freezing only from June to September, which causes lakes to become ice free and causes increases in lake water column nutrient content and light and oxygen availability (Shanahan et al., 2013; Zhao et al., 2021), in turn causing high aquatic production. Although the exact source organism(s) of lacustrine brGDGTs is still unclear, brGDGT production in Arctic lakes is higher during the ice-free season than the ice covered season (Colcord et al., 2015; Shanahan et al., 2013; Zhao et al., 2021). The brGDGT indices that can indicate production under suboxic conditions, HP5 and fractional abundance of brGDGT IIIa (%IIIa) (Weber et al., 2018; Yao et al., 2020), were high in all the study lakes from 10 to 8 ka, low between 8 and 5 ka, and gradually increasing thereafter (Fig. 2b and Fig. S6–10). In lakes Bullet, Marshall, and Pluto, correlations between Cald/Cren and both HP5 and %IIIa were not significant (Table S4), suggesting a decoupling between sub-oxic conditions inferred from isoGDGT-derived Cald/Cren and brGDGT-derived HP5 and %IIIa. In Lake N3, we observed a significant negative correlation between Cald/Cren and %IIIa, indicating antiphase sub-oxic conditions inferred from isoGDGT and brGDGT proxies (Fig. S6–S10 and table S4). In contrast, Lake Rosaea had significant positive correlations between Cald/Cren and both HP5 and %IIIa. However, the Cald/Cren ratio in Lake Rosaea remained below 45 in all samples except the last sample where ratio is <110, suggesting relatively oxic conditions, although it is possible that suboxia influenced the brGDGTs distributions in Lake Rosaea (Fig. S8). Based on the evidence for seasonal production and the contrasting trends in these lake time series, we interpret the br-and iso-GDGTs to be predominantly produced during different seasons: brGDGTs in ice-free season and isoGDGTs in ice covered season (Baxter et al., 2021; Blaga et al., 2011; van Bree et al., 2020; Loomis et al., 2014b; Shanahan et al., 2013). This contrast in seasonal production may be enhanced when caldarchaeol production is high due to winter lake water sub-oxia. In lakes N3, Pluto, and Marshall brGDGT IIIa′′ (Weber et al., 2015) is below detection limit in all samples. Lake Rosaea had brGDGTs IIIa′′ in, one Early Holocene and four Middle Holocene samples. In Lake Bullet, brGDGT IIIa′′ concentration was below detection limit prior to 7 ka. After 7 ka, concentration increased, reaching a maximum between 6 and 3 ka (Fig. S10). Afterwards, concentration remained low. The Holocene trends between Cald/Cren and IIIa′′ are decoupled with each other, while trend between IIIa′′ and HP5 and %IIIa are similar, supporting our inferences of different production seasonality of GDGTs.

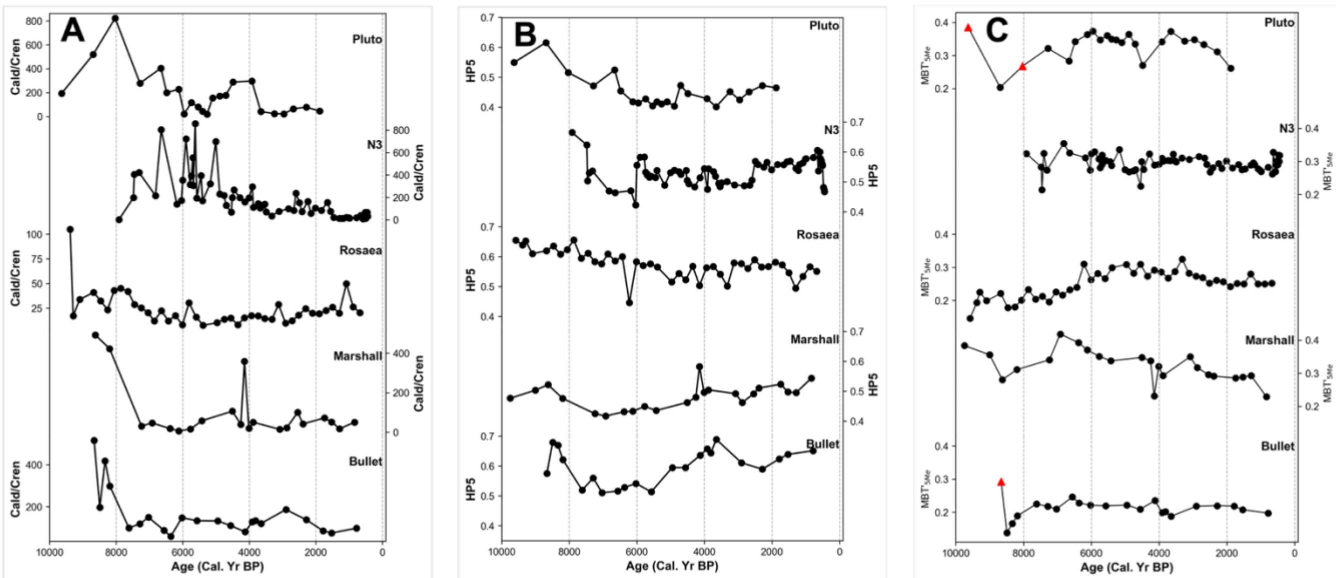

Figure 2: GDGT-based indices in study lakes. (A) Ratio of caldarchaeol to crenarchaeol (Cald/Cren) (Blaga et al., 2009), (B) Ratio of 5-methyl hexamethylated and pentamethylated brGDGTs with no cyclopentane rings (HP5) (Yao et al., 2020), and (C) Methylation of Branched Tetraethers index (MBT'_{5Me}) (De Jonge et al., 2014). Red trangles in (C) indicate samples with IR_{6Me}>0.4, which are excluded from temperature reconstructions, due to likely non-thermal influence (Bauersachs et al., 2023; Novak et al., 2025).

Lake model simulations under 30 years of modern climate suggest the occurrence of stratification (i.e., mixing depth is less than the 75% of maximum lake depth) in all the study lakes during winter and early in the ice-free season (Fig. S14), as observed today in Arctic lakes (Antoniades et al., 2024; Klanten et al., 2024; Saros et al., 2016). Sensitivity test suggests that the duration of ice-free season stratification remain constant or increases as annual or JJAS temperature increases (Fig. 3g and Fig. S14). However, the simulations show that, no matter the climate forcing, the lakes do not remain stratified throughout the entire ice-free season (Fig. 3h and Fig. S14). This means that, even if the study lakes are stratified during early spring, the lake water fully mixes during the late summer and autumn, a phenomenon observed today in Arctic lakes with similar size and chemical composition (Antoniades et al., 2024; Klanten et al., 2023, 2024; Lindborg et al., 2016). The duration of the isothermal mixing period changes similarly in all the study lakes in response to annual or JJAS air temperature model sensitivity tests, except for Lake N3 and Lake 578 (Fig. 3h and Fig. S14). In these lakes, the duration of the isothermal mixing period shows minor variations with perturbation in annual or JJAS air temperate, probably because of their larger surface area and depth compared to other study lakes. Overall, these model simulations suggest that while summer stratification does occur in these lakes, the duration of stratification is relatively short and therefore likely unable to support summer suboxic conditions, similar to Arctic lakes that experience summer stratification today (Antoniades et al., 2024; Klanten et al., 2024). The lakes in this study are relatively shallow and have low dissolved solids compared to some Arctic lakes that today experience extended summer stratification and hypolimetic sub-oxia (Saros et al., 2016), making the lakes in this study more susceptible to mixing by solar heating and wind. Winter sub-oxia would have a minimal impact on brGDGTs, which are primarily produced during the ice-free period (Loomis et al., 2014b; Shanahan et al., 2013; Zhao et al., 2021). Therefore, we assume that brGDGTs in the study lakes, mainly produced during summer, are minimally influenced by changes in sub-oxic conditions during the Holocene.

While there are several lacustrine brGDGT–temperature calibrations available globally (Martínez-Sosa et al., 2021; Raberg et al., 2021; Zhao et al., 2023), regionally (Bauersachs et al., 2023; Dang et al., 2018; Otiniano et al., 2023, 2024; Russell et al., 2018), and site-specifically (Zhao et al., 2021; Bittner et al., 2022; Feng et al., 2019), only Raberg et al. (2021), Zhao et al. (2021), and Otiniano et al. (2023; 2024) are based on the Hopmans et al., (2016) HPLC method separating GDGTs isomers and explicitly consider Arctic seasonal climate. Therefore, we assess these calibrations to infer temperature in the southwestern Greenland lakes. The Raberg et al. (2021) and Otiniano et al. (2023; 2024) calibrations estimate mean air temperature for the months above freezing (MAF) while Zhao et al. (2021) estimates epilimnion lake water temperature for the ice-free season (Ice free season lake water temperature, IFS LWT). For all analyzed samples, the reconstructed MAF based on equation 11 in Raberg et al. (2021) yields a temperature range from ~3.9 to 11.6 °C; Otiniano et al. (2024) yields a temperature range from 3.8 to 8.6 °C; and Otiniano et al. (2023) yields a temperature range from 5.8 to 9.9 °C, while IFS LWT reconstrued using Zhao et al. (2021) yields a temperature range from ~5.9 to 21.6 °C (Fig. S13). For lakes Marshall, N3, Pluto, and Rosaea, all four calibrations generated similar temperature trends throughout the Holocene, while the absolute values are different (Fig. S13). For Bullet Lake, the MBT'_{5ME}-based calibrations (Otiniano et al. (2024), Otiniano et al. (2023), and Zhao et al. (2021)) yielded similar trends, whereas Raberg et al. (2021) yielded a divergent trend, in addition to the calibrations yielding different absolute values (Fig. S13, black time series). The discrepancy between these MBT'_{5ME}-based calibrations and Raberg et al. (2021) calibration in Bullet Lake could be due brGDGTs Ib, which weighs more on Raberg et al., 2021 than MBT'_{5ME}-based calibrations, is more abundance in Bullet Lake (Fig. S11).

Observations of Arctic lakes show that water temperature changes are smaller and delayed compared to air temperature (Kettle et al., 2004; Piccolroaz et al., 2020). The lake model sensitivity tests that we conduct here, align with observations, they suggest a lake temperature response of approx. 0.4 to 0.6 °C for every 1 °C annual or JJAS air temperature change (Fig. 4 and Fig. S16). Considering this relationship between air and lake temperature responses, the Zhao et al. (2021) calibration provides an excessively high estimation of the air temperature change during the Holocene, ranging from +10 to +15 °C. The estimation of temperature of the months above freezing (MAF-T) based on Otiniano et al. (2024; 2023) and Raberg et al. (2021) are more reasonable for southwestern Greenland. Therefore, since the three calibrations are equally valid for this region, we used the average of these calibrations to estimate the MAF-T in our study lakes (Otiniano et al., 2023, 2024; Raberg et al., 2021). We estimate the error as the standard deviation between these three calibrations. Root mean square error for each calibration is 1.97 °C (Raberg et al., 2021), 1.16 °C (Otiniano et al., 2023), and 1.2 °C (Otiniano et al., 2024).

The isomer ratio of 5- to 6-methyl brGDGTs (IR_{6Me}) ranges from 0.13 to 0.51 across all study lakes (Fig. S6–10). Previously, a non-thermal effect on lacustrine brGDGTs has been identified when IR_{6Me} is greater than 0.4 (Bauersachs et al., 2023; Novak et al., 2025). In Lake Pluto two samples during the Early Holocene and in Lake Bullet the bottom sample have IR_{6Me} greater than 0.4 (Fig. 2). Consequently, all samples with IR_{6Me} greater than 0.4 were excluded from temperature reconstructions. For Lake Gus, we employed the same screening for soil-derived brGDGTs (excluding all samples with <30% hexa-methylated GDGTs) as used in Cluett et al., (2023).

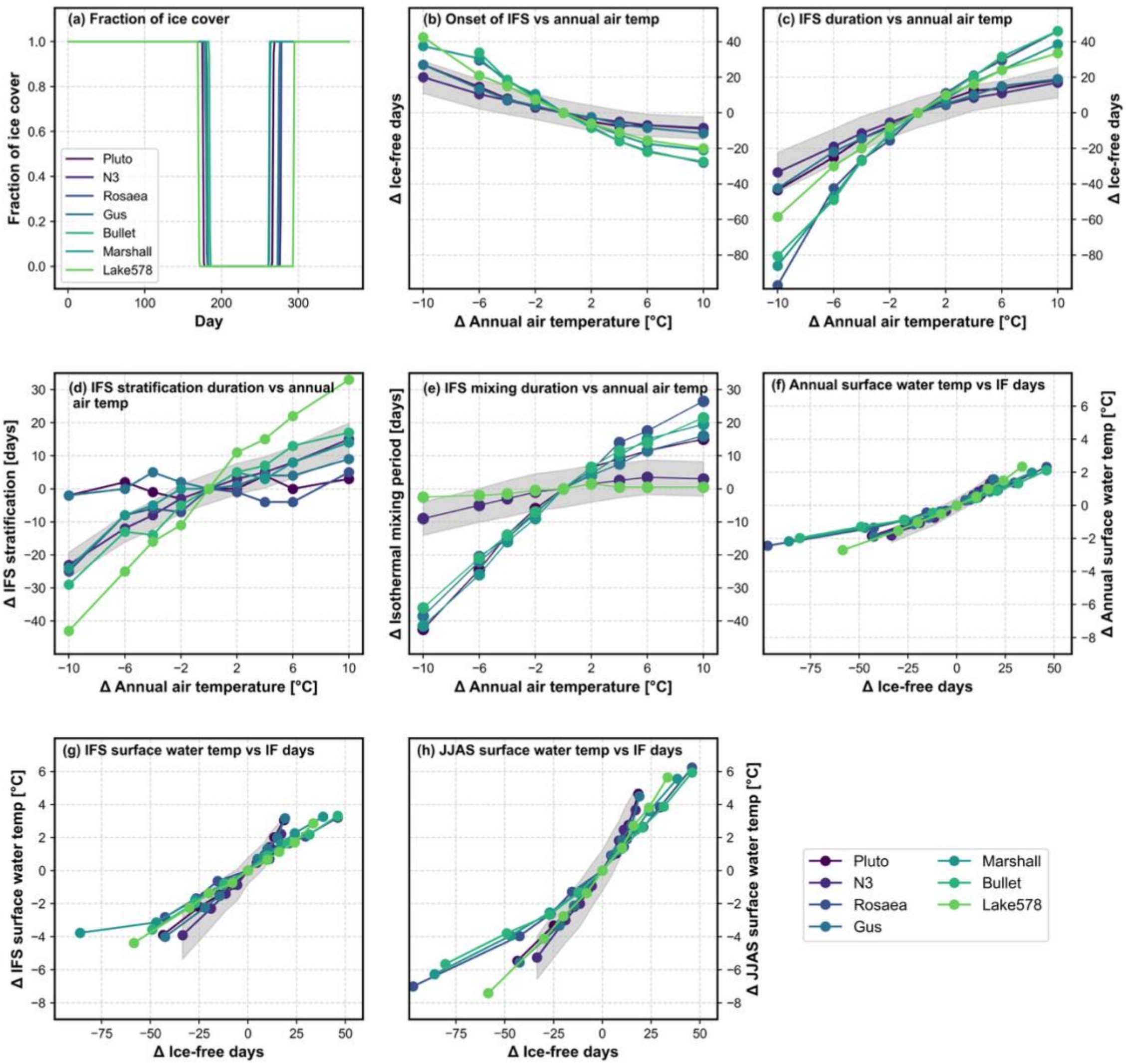

Figure 3: Simulations of fraction of ice cover, duration of ice-free season (IFS), surface water temperature, IFS stratification, and IFS mixing period. (a) Simulations of the fraction of the lake covered by ice in study lakes. Line is the median value of the 30-year simulation under modern climate. (b) to (h) Sensitivity tests where annual temperature was changed, shown as anomalies relative to the simulation under modern climate. Each point denotes the median value of the 30-year simulation. Gray shading represents the standard deviation for the 30 years simulated for Lake N3. Standard deviation is on the same order for other lakes. (b) to (e) Response of lake ice-cover and mixing dynamics to changes in annual air temperature. (b) Onset date of ice-free conditions. (c) IFS duration. (d) IFS stratification duration (stratification defined as mixing depth less than 75% of maximum lake depth). (e) IFS isothermal mixing duration (defined as mixing depth greater than 75% of maximum lake depth). (f) to (h) Relationship between IFS duration and lake surface water temperature averaged across (f) the entire year (g) the IFS and (h) JJAS.

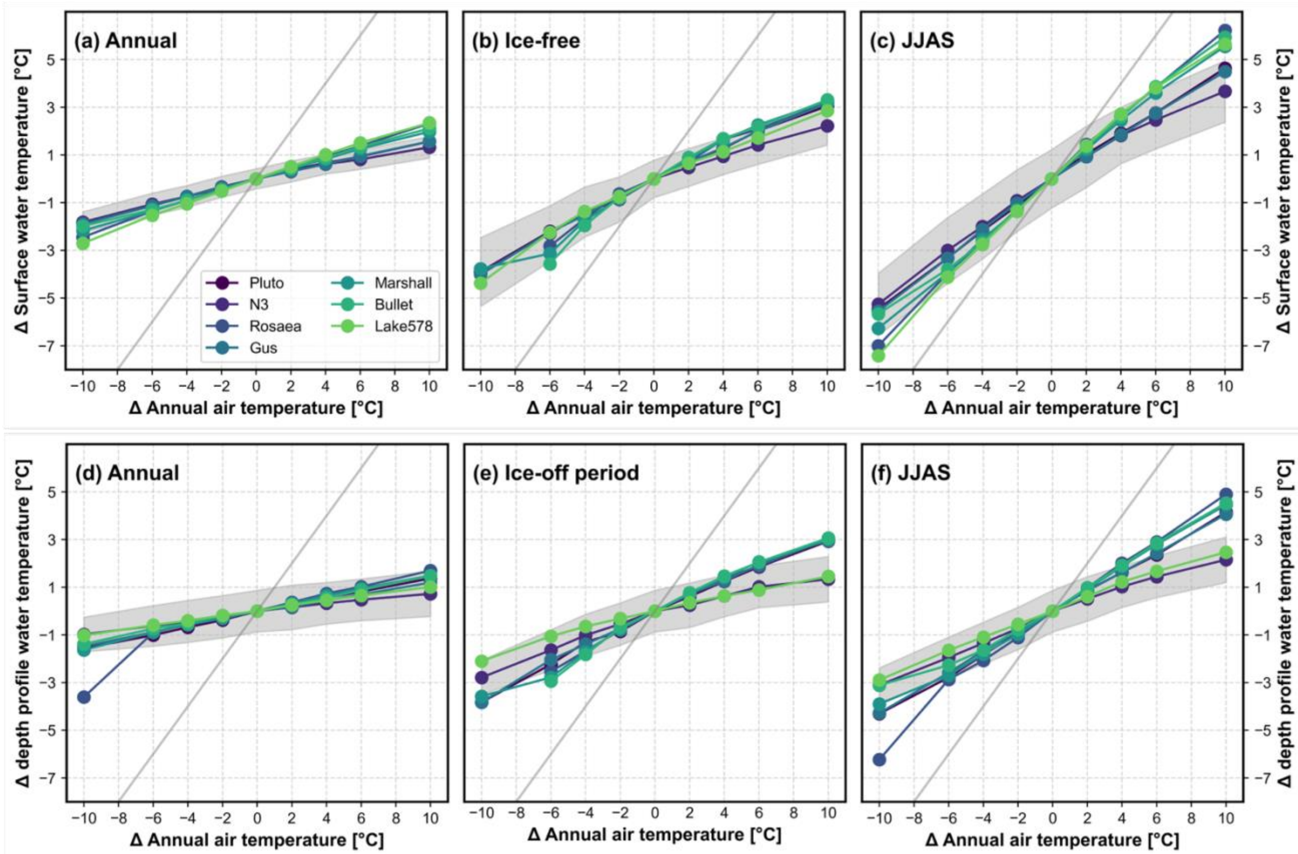

Figure 4: Sensitivity of surface water (a–c) and average depth profile temperatures (d–f) to changes in annual air temperature. (a) and (d) annual, (b) and (e) IFS, (c) and (f) JJAS water temperature [°C]. Each point denotes the median value of the 30-year simulation. Gray line is the 1:1 line. Gray shading represents the standard deviation for the 30 years simulated for Lake N3. Standard deviation is on the same order for other lakes.

3.2 Holocene temperature variability

Reconstructed MAF-T shows both similarities and differences between time series, with differences not following a latitudinal gradient. Reconstructed MAF-T varies from 5.9 to 9.6 °C for Pluto, 6.2 to 9.2 °C for N3, 4.8 to 8.4 °C for Rosaea, 6.1 to 9.7 °C for Marshall, and 4.5 to 8.1 °C for Bullet, respectively (Fig. 5). In lakes Pluto and Bullet, the temperature timeseries start at approx. 9 ka, and reveal a trend towards warm conditions (Fig. 5a). In lakes Marshall and Rosaea, the temperature timeseries begin from approx. 9.5 ka, with warm conditions indicated in Marshall Lake, while cold conditions prevail in Lake Rosaea (Fig. 5b and c). In Marshall Lake, temperature decreased around 8 ka and then increased, peaking at approx. 7 ka. In Lake N3, the temperature timeseries begins at 8 ka and reveals warm conditions. In lakes N3, Marshall, and Pluto the maximum temperature occurred between 7.5 to 5 ka (Fig. 5). Immediately following the peak warmth, MAF-T in these three lakes reveals a gradual cooling trend until approx. 4.5 ka, followed by warm conditions until 3 ka, then gradual cooling. In Bullet Lake, the temperature trends are muted compared to the other lakes, perhaps in part because the three calibrations yield contrasting trend (Fig. S13, black lines). The temperature maximum began at the same time as these other sites, around 8 ka, but lasted longer, until 2 ka, followed by cooling. Overall, the pattern of reconstructed MAF-T from Pluto, N3, Bullet, and Marshall lakes, spanning 5° latitude in southwestern Greenland, is similar to the annual temperature reconstruction from Greenland Ice Sheet Project 2 ice core (Fig. 6b), albeit with differences likely caused by spatio-temporal variation and resolution of the timeseries (Kobashi et al., 2017). Furthermore, the long-term temperature trends observed in N3, Pluto, and Marshall lakes is comparable to brGDGT-inferred MAF-T timeseries from Lake Gus (Cluett et al., 2023) and Lake 578 (Schneider et al., 2024) (Frechette and de Vernal, 2009) (Figs. 5 and 6).

In contrast to the other timeseries, the reconstructed temperature in Lake Rosaea reveals consistent cool conditions from 9 to 7 ka, warming from 7 to 5 ka, and peak warmth between approx. 5 and 3 ka, lagging by two millennia peak warmth inferred from brGDGTs at six other southwestern Greenland lakes (Fig. 5b). This delayed peak warmth is synchronous with a biogenic silica record from Qipisarqo lake (Fig. 6i) (Kaplan et al., 2002) and pollen-based records from southern Greenland (not shown) (Frechette and de Vernal, 2009; Fredskild, 1973; Gajewski, 2015). Next, we discuss possible mechanisms explaining this temporal discrepancy in thermal maxima.

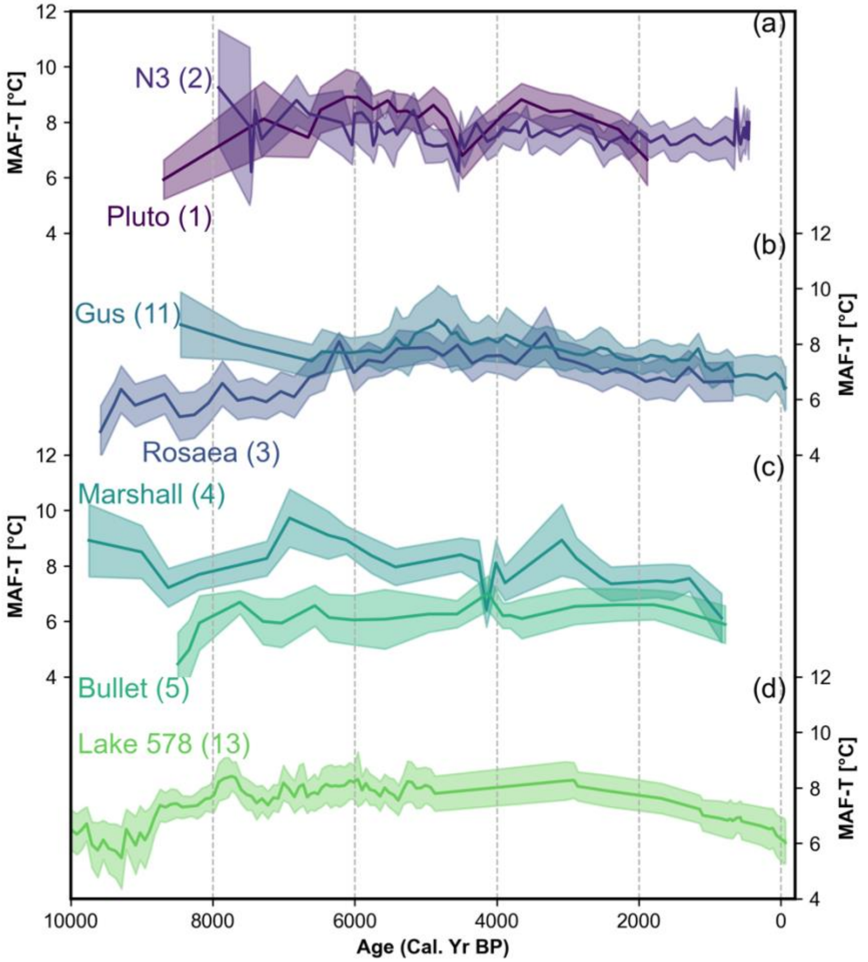

Figure 5: Reconstructed mean air temperatures of the months above freezing (MAF-T) in (a) Lakes N3 and Pluto at 69 °N, (b) Lakes Gus (Cluett et al., 2023) and Rosaea at 67 °N, (c) Lakes Marshall and Bullet at 64 °N, and (d) Lake 578 at 61 °N (Schneider et al., 2024). Bold lines indicate average MAF-T inferred from three high-latitude lacustrine brGDGTs calibrations (Otiniano et al., 2023, 2024; Raberg et al., 2021), and shading represents standard deviation of these calibrations. Numbers in parentheses next to site names refer to site IDs shown in Fig. 1.

3.3 Possible mechanisms causing temporal differences in peak warmth among time series on western Greenland

BrGDGT-inferred MAF-T timeseries from southwestern Greenland reveal lower absolute value and magnitude of temperature change at Lake Bullet and a delayed thermal maximum at Lake Rosaea, compared to the other lakes. To interpret these variations, we explored potential mechanisms influencing the brGDGT timeseries from the seven lakes in southwestern Greenland.

3.3.1 Production period of brGDGTs

Lake ice regulates the availability of nutrients, light, and oxygen, thereby influencing the production period of bacteria producing brGDGTs. Therefore, the duration and timing of the ice-free season can influence the production period of brGDGTs (Loomis et al., 2014a; Miller et al., 2018). Simulations of all the study lakes under 30 years of modern climate suggest that all lakes exhibit < 2-week inter-lake variations in the timing of the onset of the ice-free season (Fig. 3a). Duration of the ice-free season is approx. <20 days shorter in lakes Bullet and Marshall, probably due to their higher elevation, and approx. 20 days longer in Lake 578 than lakes Pluto, N3, Gus, and Rosaea (Fig. 3a). Additionally, both the onset date and duration of the ice-free season respond similarly in all seven lakes to perturbations in annual air temperature (Figs. 3b– c). Annual, ice-free season and JJAS surface water temperature of all the lakes vary similarly with changes in duration of the ice-free season (Figs. 3d – e). These results suggest that the temperature response of studied lakes to the same forcing is similar, and therefore if brGDGTs are produced during the ice-free season, their temperature response should be similar among lakes if atmospheric temperature change is similar.

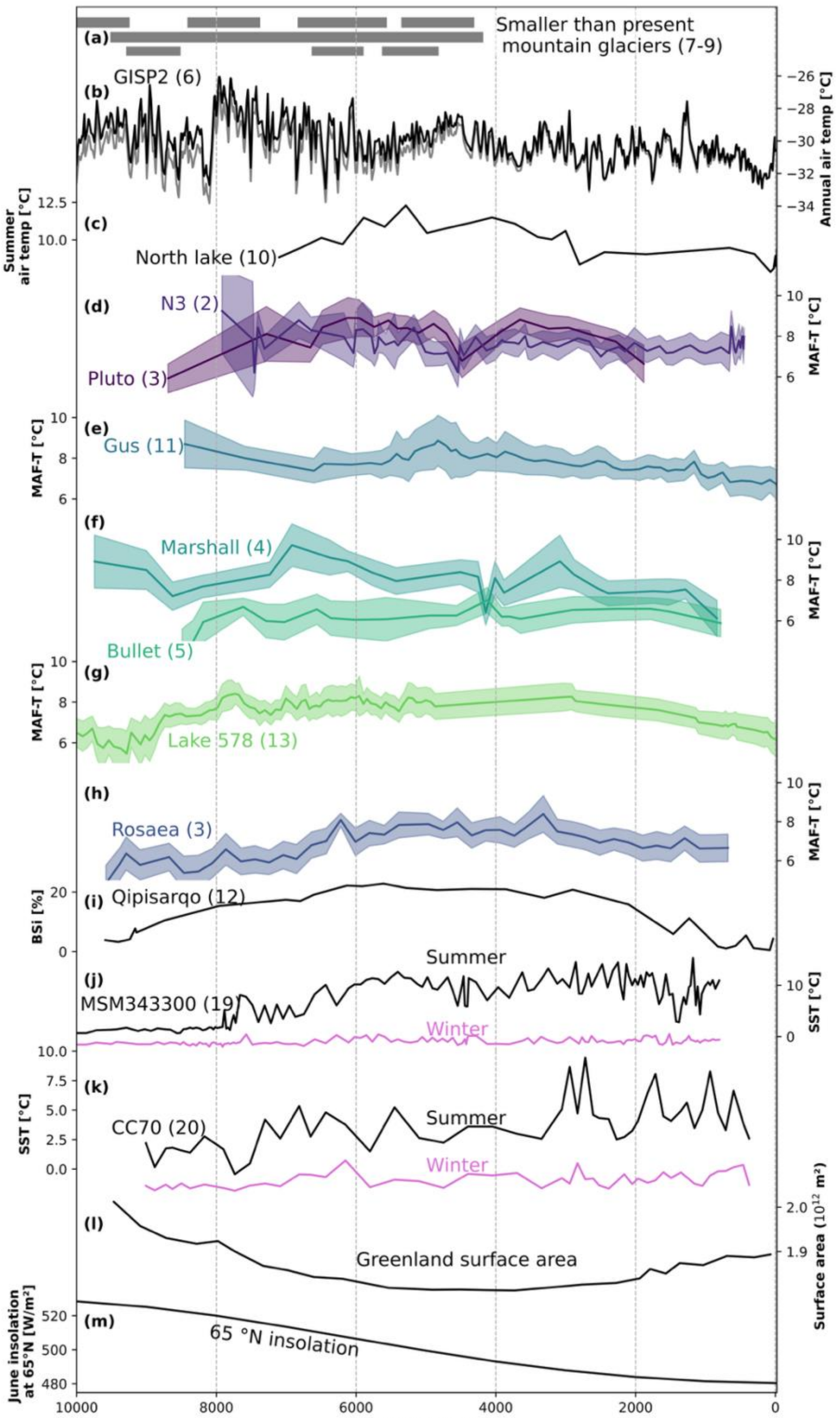

Smaller than present mountain glaciers (7-9)
(a)
(b)
GISP2 (6)
Annual air temp [°C]
(c)
Summer air temp [°C]
North lake (10)
(d)
N3 (2)
Pluto (3)
MAF-T [°C]
(e)
Gus (11)
MAF-T [°C]
(f)
Marshall (4)
Bullet (5)
MAF-T [°C]
(g)
Lake 578 (13)
MAF-T [°C]
(h)
Rosaea (3)
MAF-T [°C]
(i)
Qipisarqo (12)
BSi [%]
(j)
MSM343300 (19)
Summer
Winter
SST [°C]
(k)
CC70 (20)
Summer
Winter
SST [°C]
(l)
Greenland surface area
Surface area (10^{12} m²)
(m)
65 °N insolation
June insolation at 65°N [W/m²]
Age (Cal. Yr BP)

Figure 6: Holocene temperature history from southwestern Greenland. (a) Smaller-than-present mountain glaciers (Schweinsberg et al., 2017, 2019), (b) Annual air temperature [°C] inferred from gas fractionation from Greenland Ice Sheet Project 2 ice core, with the black line indicating elevation corrected values and the grey line indicating elevation uncorrected values. (Axford et al., 2021; Kobashi et al., 2017), (c) chironomid-inferred July air temperature [°C] from North Lake (Axford et al., 2013), brGDGT-inferred mean air temperatures for months above freezing (MAF-T) [°C] from (d) lakes N3 and Pluto (This study), (e) Lake Gus (Cluett et al., 2023), (f) lakes Marshall and Bullet (This study), brGDGT-inferred MAF-T [°C] from (g) Lake 578 (Schneider et al., 2024), (h) Lake Rosaea (This study), (i) Biogenic silica as an indicator of temperature from Lake Qipisarqo (Kaplan et al., 2002), Dinocyst-inferred sea surface temperatures (SST) [°C] from (j) Disko Bugt core MSM343300 (Ouellet-Bernier et al., 2014), and (k) Baffin Bay core CC70 (Gibb et al., 2015) (l) Greenland Ice Sheet surface area (*10^{12}) [m^2] (Larsen et al., 2015) and (m) 21st June insolation at 65 °N [W m^{-2}] (Laskar et al., 2004). Numbers in parentheses next to site name refer to site IDs shown in Fig. 1.

3.3.2 Sensitivity of lake system

Similar to the onset and duration of the ice-free season, the response of lake water temperature during the ice-free season may vary among study lakes due to their different morphological characteristics and thermodynamics. Yet, lake model simulation reveals that the annual, IFS, and JJAS surface water temperatures of the seven lakes exhibit similar responses to changes in annual air temperature (Fig. 4). The lake model exhibited a similar, but slightly muted, response to JJAS air temperature perturbations (Fig. S16). This result suggests that despite morphological differences, the surface water temperature of the studied lakes, is equally sensitive to changes in air temperature. Since brGDGTs in lakes can be produced in surface waters, water columns, and/or sediment (Acharya et al., 2023; Buckles et al., 2014; Yao et al., 2020; Zhao et al., 2021), we also examined the response of the average depth profile temperature of the lakes to perturbations in annual and JJAS air temperature (Fig. 4 d–f and Fig. S16 d–f). As with the surface temperature, all the lakes exhibit similar responses, except lakes N3 and 578, which has a slightly muted response compared other lakes, especially in the JJA temperature profile, probably caused by greater maximum depth compared to other lakes. Therefore, the greater depth of lakes N3 and 578 may have led to slightly lower-amplitude (approx. <1 °C) Holocene temperature variations compared to the other lakes (Fig. 5). However, several millennia of delayed thermal maximum in Lake Rosaea and approx. 2 °C lower absolute temperatures in Bullet Lake compared to other lakes cannot be explained by sensitivity to air temperature forcing.

3.3.3 North-South pattern in timing of temperature maxima

To explore the north-south pattern in the timing of temperature maxima, we compared all the available brGDGT-based temperature reconstructions from southwestern Greenland including from Lake Gus (Fig. 1; point 11) (Cluett et al., 2023) and Lake 578 (Fig. 1; point 13) (Schneider et al., 2024). Together these seven lakes cover the latitudinal gradient from ~61°N to 69°N (Table 1). If we assume a north-south pattern in the timing and magnitude of the temperature maxima caused by Arctic Amplification (Axford et al., 2021; Briner et al., 2016; Kaufman, 2004), the lakes at the highest latitudes in the transect (Pluto and N3) should exhibit higher magnitude and earlier temperature maxima compared to lakes at lower latitudes (Rosaea and Gus, 67°N; Marshall and Bullet 64°N; and 578, 61°N). However, the timing of the temperature maximum at the southernmost site, Lake 578 (8 to 5 ka) is similar to that of lakes N3 and Pluto at 69 °N and Lake Marshall at 64 °N, occurring between *ca.* 7.5 to 5 ka (Fig. 5). Moreover, Lake Bullet, situated at a similar latitude to that of Lake Marshall, exhibits a prolonged temperature maximum between *ca.* 8 to 2 ka. The time series that shows a delayed temperature maximum, between *ca.* 5 and 3 ka, occurs in the middle of the transect: at Lake Rosaea (67°N). This delayed timing in temperature maximum at Lake Rosaea is not observed in the timeseries from Lake Gus, at the same latitude, where peak temperatures occurred between *ca.* 9 to 5 ka (Cluett et al., 2023). A similar thermal maximum timing among six of the seven brGDGT timeseries from southwestern Greenland suggests that Arctic Amplification was not the primary mechanism setting the timing of peak warmth in this region. In addition, Lake Rosaea must be primarily responding to different primary forcing mechanisms than the other lakes.

3.3.4 Ice-sheet and ocean proximity

Lakes Bullet and Marshall are <2 km distance to the margin of the modern Greenland Ice Sheet, whereas lakes N3, 578, and Pluto are > 10 km, and lakes Gus and Rosaea are > 100 km away (Table 1). Deglaciation from lakes Gus, Rosaea, Marshall, Bullet, and 578 occurred before 10 ka (Leger et al., 2024). The margin of the Greenland Ice Sheet was relatively stable from 9 to 6 ka near lakes Marshall, Bullet, and 578, while it was receding inland from lakes Rosaea and Gus. Since 9 ka, the margin of the ice sheet was always at least 50 km inland from lakes Rosaea and Gus. By contrast, lakes N3 and Pluto deglaciated at ~8 ka (Leger et al., 2024; Young et al., 2013) and the margin of the Greenland Ice Sheet was <3 km aerial distance from these lakes until 7.5 ka. The margin of the southwestern Greenland Ice Sheet retreated inland of its present-day margin around 6 ka and returned to its present margin around 1850 AD (Leger et al., 2024), although the little available evidence suggests the retreat was <10 km (Briner et al., 2014; Cronauer et al., 2016; Lesnek et al., 2020). This suggests that lakes Bullet, Marshall, Pluto, and N3 could have been significantly influenced by the proximity of the ice sheet during the Holocene, while Lakes Rosaea and Gus are minimally influenced, and Lake 578 might be moderately influenced. Thus, the fact that peak warmth occurred after 8 ka, following ice sheet retreat from Lakes Marshall, Bullet, N3, and Pluto suggests that the ice sheet may have kept local conditions cold. However, Marshall Lake experienced moderately warm conditions at 9 ka, a period that most of these other timeseries do not capture, suggesting that ice-sheet proximity may not have been the primary factor influencing MAF-T at these lakes. Lake Rosaea is an obvious outlier in this ice-sheet proximity pattern: it was far from the ice sheet for most of the Holocene, so should be minimally influenced by katabatic winds, but has a low magnitude of temperature change and the latest thermal maximum of all the records. Thus, temperature at Lake Rosaea is likely not influenced by its distance from the Greenland Ice Sheet.

Ocean conditions influence coastal climate by affecting ocean-atmosphere heat transfer (Bashmachnikov et al., 2023). A warmer ocean releases heat into the atmosphere, resulting in warmer coastal climates, and vice versa with cold ocean conditions. Lakes Bullet and Marshall are ≥100 km and lakes 578 and Gus are >60 km from the open ocean (Table 1). Thus, the ocean influence on these lakes is likely minimal. Lakes N3, Pluto, and Rosaea are situated near the ocean (<3 km). Modern wind directions at Lake Rosaea are predominantly southerly, meaning that most airmasses at Lake Rosaea come directly from the Labrador Sea and Davis Strait (Fig. 7a). About 20% of winds at Lake Rosaea are northerly, meaning they pass over Baffin Bay prior to arriving at Lake Rosaea. In contrast, at lakes Pluto and N3, wind direction is more variable, meaning that half of the airmasses originate from land and half from Disko Bugt (Fig. 7a). The pattern of reconstructed lake water temperature from Lake Rosaea is similar to summer sea surface temperature (SST) timeseries from Disko Bugt and Baffin Bay (Fig. 6j, k), as well as other North Atlantic SST time series, which reach maxima in the Middle and Late Holocene (Gibb et al., 2015; Hansen et al., 2020; Ouellet-Bernier et al., 2014; Saini et al., 2022). This similarity implies that temperature at Lake Rosaea is more strongly influenced by oceanic conditions via ocean-atmosphere heat exchange than the other lakes in this transect. Summer SSTs in eastern Baffin Bay were cold during the Early Holocene, probably caused by meltwater from the rapidly retreating Greenland Ice Sheet and a weaker western Greenland current (Gibb et al., 2015; Hansen et al., 2020). SSTs rose during the middle-Holocene related to decreased meltwater from the Greenland Ice Sheet and increased influence of warm Atlantic water masses (Ouellet-Bernier et al., 2014; Perner et al., 2013). The reconstructed temperature pattern from Lakes Pluto and N3 exhibits a closer resemblance to the lakes that are far from the ocean. These lakes may have been less affected by Holocene Ocean conditions than Lake Rosaea due to local topography, including proximity to the ice sheet and their position in interior Disko Bugt.

3.3.5 Topographic conditions

Steep topography surrounding a lake can shade the lake, influencing the direct short-wave radiation reaching lake surface, thereby regulating the lake surface water temperature. To investigate the mechanisms for the differences in absolute temperature and magnitude of Holocene temperature variations in the five study lakes, we examined the topographic conditions around each lake. Shading calculations show that of the five lakes, Pluto Lake is the least shaded by surrounding topography and Bullet Lake is the most shaded (15% less direct shortwave radiation than Pluto Lake) (Fig. 7b). Lakes N3 and Marshall are approx. 5% more shaded than Pluto Lake, whereas Lake Rosaea is 10% more shaded than Pluto Lake (Fig. 7b). This means that the topography surrounding lakes N3, Marshall, Rosaea, and Bullet cause them to receive correspondingly less solar radiation compared to Pluto, with Bullet receiving the least. We assess the impact of shading on lake water thermodynamics by perturbing the magnitude of incoming shortwave radiation in the lake model. These simulations suggest that a 10% decrease in incoming short-wave radiation can suppress the mean ice-free season lake surface temperature by approx. 1.5 °C and a 25% decrease by 4 °C (Fig. 7c). Therefore, we suggest that the slight (~1–2 °C) difference in absolute temperature values between the lakes Pluto, N3, Marshall and Rosaea could be related to local topography and variations in incoming shortwave radiation to the lakes. Approx. 2 °C lower absolute temperature and approx. 0.5 °C lower magnitude of temperature change in Bullet Lake may be due to lowest incoming shortwave radiation, compared to the other study lakes. There may also be other factors causing differences between these time series, but we believe we have assessed the primary mechanisms here.

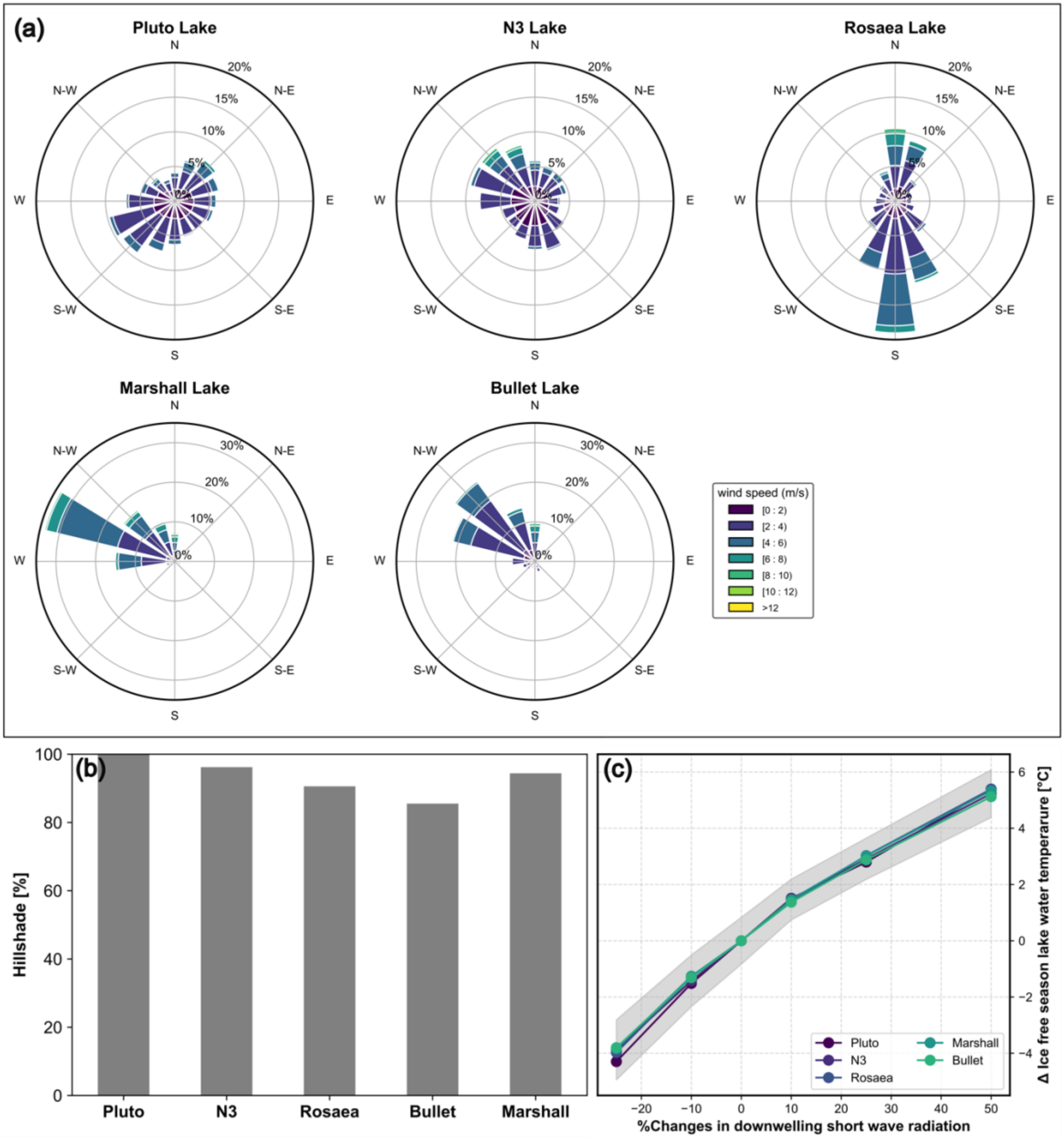

Figure 7: (a) Wind strength and direction in the study lakes from April to September, based on six-hourly ERA5 data from 1994 to 2024. (b) Percentage change in average summer (April to September) direct radiation on study lakes relative to Pluto Lake, which is the least shaded of the five. (c) Sensitivity of average surface water temperature to changes in incoming shortwave radiation. Each point denotes the median value of the 30-year simulation. Gray shading represents the standard deviation for the 30 years simulated for Lake N3. Standard deviation is on the same order for other lakes.

4 Holocene temperature history of southwestern Greenland

The majority of brGDGT-inferred MAF-T timeseries from southwestern Greenland (N3, Pluto, Marshall, Bullet and 578) document peak warmth in the Middle Holocene, between *ca.* 7 and 5 ka, following maximum summer insolation. Timeseries from Lake Gus reveal peak warmth between *ca.* 9 to 6 ka, earlier than many other time series. An earlier deglaciation at Lake Gus (before ca. 10 ka), and minimal influence from the Greenland Ice Sheet and coast during the Holocene, likely have caused earlier warmth. However, ~25 samples from the Early Holocene in Lake Gus were removed due to evidence of high input of soil-derived brGDGTs (Cluett et al., 2023), so it is possible that other samples in that section have some minor influence of soil-derived brGDGTs, causing elevated inferred MAF-T. The timeseries from Lake Marshall shows warmth at *ca.* 9 ka, followed by cooling *ca.* 8 ka and subsequent warming, similar to the regional ice-sheet retreat rate reconstructions (Lesnek et al., 2020), suggesting this timeseries captured Early Holocene warm conditions not captured in most lake records, since they start later. Immediately after peak warmth, temperature reconstructions in all study lakes show a gradual cooling trend towards the Late Holocene. This pattern of temperature change can also be inferred from alpine glacier reconstructions from throughout southwestern Greenland, which experienced high retreat rates or completely disappeared during the Early Holocene and reappeared during the Late Holocene (Fig. 6a) (Larocca et al., 2020; Larsen et al., 2017; Lasher et al., 2020; Schweinsberg et al., 2017, 2019). Furthermore, Holocene vegetation in southwestern Greenland indicates the warmest summer conditions in the Holocene between 7.2 and 6.3 ka, followed by cooling (Fredskild, 1983), a pattern similar to timeseries from lakes N3, Pluto, Marshall, and Bullet and 578 (Schneider et al., 2024). Similarly, occurrence of warmth-demanding ostracodes in lake sediments at the head of Kangerlussuaq (inland from Lake Gus) indicates peak Holocene summer temperatures from c. 7.0 to 6.5 ka (Bennike et al., 2010). The Early Holocene peak warmth and the subsequent cooler Late Holocene documented by the most of these new brGDGTs-derived time series and other summer-sensitive proxy time series in southwestern Greenland align with the temperature pattern observed in many proxy time series from Greenland and Arctic Canada, albeit with spatial and temporal variability (Axford et al., 2021; Briner et al., 2016; Kaufman, 2004; Larocca and Axford, 2022).

Lake Rosaea experienced a thermal maximum between approx. 5 to 3 ka, coinciding with nearby SST reconstructions (Fig. 4j, k) (Gibb et al., 2015; Ouellet-Bernier et al., 2014). Similarly, the biogenic silica (BSi) record from Lake Qipisarqo (Fig. 3i), pollen-based reconstructions from Lakes Comarum Cø, and Kløft Sø, all coastal sites that are influenced by the East Greenland Current, reveal a delayed thermal maximum, after 6 ka, in accord with marine temperature timeseries (Fig. 3j, k) (Andresen et al., 2004; Fredskild, 1973; Gajewski, 2015; Kaplan et al., 2002). This suggests the influence of ocean conditions on coastal temperatures via ocean-atmosphere heat exchange.

The magnitude of peak warmth in brGDGT-inferred MAF-T show both similarities and differences between time series. BrGDGT-inferred MAF-T timeseries from lakes Pluto, N3, Gus, Rosaea, and 578 show on average 1.0 ± 0.5 °C higher temperatures during the peak warmth (from 7 to 5 ka) relative to average between 2 ka to the present. Marshall Lake shows approx. 0.7 °C higher temperatures compared to the other lakes. The relatively warmer temperature in Marshall Lake is likely due to its higher elevation, which would have caused higher rate of warming (Pepin et al., 2015). Lake Bullet shows relatively stable temperatures over the Holocene, perhaps due to lowest incoming shortwave radiation, compared to the other study lakes, although uniquely contrasting trends among the three brGDGT-temperature calibrations for the Lake Bullet time series may also explain the relative lack of trend. Overall, the magnitude of peak warmth in lakes Pluto, N3, Gus, Marshall, and Bullet are lower than the chironomid-inferred July air temperature from North Lake showing 2 – 3°C warmer conditions between 7 and 5 ka relative to average between 2 ka to the present (Axford et al., 2013). This difference in magnitude is likely related to seasonality of reconstructed temperature (July for Chironomids, months above freezing for brGDGTs) (Eggermont and Heiri, 2012). The strongest solar radiation in July caused the higher magnitude of warming compared to the MAF-T. Further, the magnitude of peak warmth in lakes Pluto, N3, Gus, Rosaea, and 578 is lower than the ice sheet elevation change corrected annual air temperature [°C] inferred from gas fractionation from GISP2 ice core demonstrating ~1.3°C warmer conditions from 7 to 5 ka relative to the 2 to 0 ka average (Axford et al., 2021; Kobashi et al., 2017). This is surprising as the Holocene annual air temperature show a lower warming than the MAF-T (Axford et al., 2021; Briner et al., 2016). The higher magnitude of Holocene peak warmth in mean annual air temperate in GISP2 and MAF-T in lakes Pluto, N3, Gus, Rosaea, and 578 could be due higher elevation of GISP2 causing higher summer warming during peak warmth, than the coastal Greenland leading to overall higher magnitude of mean annual air temperature change in GISP2. Further investigation of proxy time series considering seasonality of temperature change and covering a wider spatial range across over the Greenland may help to reconcile these differences.

Although there are differences in timing and magnitude of peak warmth in brGDGT-inferred MAF-T timeseries for southwestern Greenland, these timeseries do not follow a latitudinal pattern. This is surprising, considering the pronounced warming in higher latitudes compared to low latitudes due to local feedbacks and remote teleconnections observed during the past century (England et al., 2021; Sweeney et al., 2023) and during the Holocene (Axford et al., 2021; Briner et al., 2016; Kaufman, 2004). The absence of Arctic Amplification in southwestern Greenland brGDGT-inferred from MAF-T timeseries in the past 9 ka could be because of several factors: (1) the latitudinal gradient across the study sites may be too small to observe temperature differences using this proxy; (2) the temporal resolution of the time series may be too coarse to detect subtle shifts in the timing of the thermal maximum; or (3) other local or regional influences, including strong ocean and atmosphere northward heat transport (Dufour et al., 2016) and the absence of Holocene summer sea ice in this region (Gibb et al., 2015), which may have been overprinted the expected signal from Arctic amplification. Future high-resolution proxy timeseries covering a larger latitudinal range and using the same proxy, reflecting similar seasonality, could help test this hypothesis.

5 Summary and conclusions

We compare five new (from Pluto, N3, Rosaea, Marshall, and Bullet Lake) and two published (from Gus Lake and Lake 578) brGDGT-inferred MAF-T time series spanning the past 9 ka from southwestern Greenland. The timeseries from lakes Pluto, N3, Marshall, Bullet, and 578 have similar trends, with temperature maxima between *ca.*7 and 5 ka, 1.0 ± 0.5 °C higher temperatures relative to the 2 to 0 ka average, and then gradual cooling towards the Late Holocene, similar to the many other regional timeseries, following maximum annual insolation at 65 °N. The timeseries from Lake Gus reveals peak warmth between *ca.* 9 to 6 ka, earlier than many other time series, likely due to minimal influence from the coast and the Greenland Ice Sheet. The time series from Lake Marshall suggests a warm Early Holocene, cooling around 8 ka and subsequent warming, which is similar to the few available proxy records of Early Holocene temperature in the ice-free margins of Greenland (Lesnek et al., 2020).

In contrast to the other timeseries, Lake Rosaea reveals a temperature maximum between ca. 5 and 3 ka, lagging peak warmth in other timeseries by two millennia. Lake model simulations suggest that proxy systematics, i.e., the production season of brGDGTs and the sensitivity of each lake system to climate changes, likely did not cause these temporal differences. Moreover, we do not observe a north-south trend in the timing of the thermal maximum in southwestern Greenland. Instead, the timing of peak warmth seems to be related to regional-scale factors: proximity to the ice sheet and ocean. Lake Rosaea is situated at the coast, with prevailing southerly winds from the ocean. Holocene temperature change at Lake Rosaea is synchronous with regional marine timeseries that indicate weaker West Greenland Current and cooler summer ocean conditions during the Early and middle Holocene caused by melt water from Greenland Ice Sheet (Axford et al., 2021; Gibb et al., 2015; Hansen et al., 2020; Ouellet-Bernier et al., 2014). Temperature at Lake Rosaea rose during the middle-Holocene when SSTs increased, due to decreased melt water flow from the Greenland Ice Sheet, which reached its minimum extent around 5 to 3 ka (Briner et al., 2014) and increased influence of warm Atlantic water masses (Gibb et al., 2015; Hansen et al., 2020; Ouellet-Bernier et al., 2014). Similar to Lake Rosaea, proxy timeseries from other coastal sites, including Lake Qipisarqo, Camarum Sø, and Kløft Sø, show a delayed thermal maximum, in accord with SST timeseries (Frechette and de Vernal, 2009; Fredskild, 1973; Gajewski, 2015; Kaplan et al., 2002). We therefore suggest that temperature reconstructions from coastal sites where prevailing winds are onshore may be strongly influenced by ocean conditions via ocean-atmosphere heat exchange.

Overall, brGDGT-inferred MAF-T timeseries suggest that local variations in temperature, influenced by the proximity to the ice sheet and ocean, caused discrepancies in timing and magnitude of Holocene temperature in southwestern Greenland. The seasonality (e.g., MAF, summer, annual) of reconstructed temperature seems important when comparing the magnitude of Holocene temperature change between the timeseries using different proxies. Therefore, further investigation of proxy time series to quantify seasonal variability and the impact of local factors, e.g., site-specific, topographic, ice sheet proximity, and oceanic conditions, will likely reveal broad similarities among proxy timeseries, helping to reconcile differences and refine Holocene climate reconstructions.

Data availability

All the data will be available at National Centers for Environmental Information for Paleoclimatology data portal.

Authors contribution

We thank the people of Greenland for providing access to their Land. The study was conceptualized by SA and EKT. AC, ALG, and ISC conducted the laboratory analysis. SA and EKT prepared the manuscript with contributions from all co-authors.

Competing interests

The authors declare that they have no conflict of interest

Acknowledgements

We thank John Ryan-Henry, Kayla Hollister, Owen Cowling, Nancy Leon, and Jeff Salacup for their help in lipid biomarker analysis. We gratefully acknowledge Dr. Gerard A. Otiniano and Dr. Samuel Mark for discussions.

Financial support

This research was funded by National Science Foundation grant OPP-1504267 and OPP-2106971 to EKT and JPB, EAR-IF 1652274 to EKT and NSF Graduate Research Fellowship 1645677 to AAC.

References

Acharya, S., Zech, R., Strobel, P., Bliedtner, M., Prochnow, M., and De Jonge, C.: Environmental controls on the distribution of GDGT molecules in Lake Höglwörth, Southern Germany, Organic Geochemistry, 186, 104689, 2023.

Andresen, C. S., Björck, S., Bennike, O., and Bond, G.: Holocene climate changes in southern Greenland: evidence from lake sediments, Journal of Quaternary Science, 19, 783–795, https://doi.org/10.1002/jqs.886, 2004.

Antoniades, D., Klanten, Y., Cameron, E., Garcia-Oteyza, J., Oliva, M., and Vincent, W. F.: Evidence of summer thermal stratification in extreme northern lakes, Arctic Science, 10, 225–232, https://doi.org/10.1139/as-2023-0037, 2024.

Axford, Y., Losee, S., Briner, J. P., Francis, D. R., Langdon, P. G., and Walker, I. R.: Holocene temperature history at the western Greenland Ice Sheet margin reconstructed from lake sediments, Quaternary Science Reviews, 59, 87–100, https://doi.org/10.1016/j.quascirev.2012.10.024, 2013.

Axford, Y., De Vernal, A., and Osterberg, E. C.: Past Warmth and Its Impacts During the Holocene Thermal Maximum in Greenland, Annu. Rev. Earth Planet. Sci., 49, 279–307, https://doi.org/10.1146/annurev-earth-081420-063858, 2021.

Bashmachnikov, I. L., Raj, R. P., Golubkin, P., and Kozlov, I. E.: Heat Transport by Mesoscale Eddies in the Norwegian and Greenland Seas, Journal of Geophysical Research: Oceans, 128, e2022JC018987, https://doi.org/10.1029/2022JC018987, 2023.

Bauersachs, T., Schubert, C. J., Mayr, C., Gilli, A., and Schwark, L.: Branched GDGT-based temperature calibrations from Central European lakes, Science of The Total Environment, 167724, https://doi.org/10.1016/j.scitotenv.2023.167724, 2023.

Baxter, A. J., van Bree, L. G. J., Peterse, F., Hopmans, E. C., Villanueva, L., Verschuren, D., and Sinninghe Damsté, J. S.: Seasonal and multi-annual variation in the abundance of isoprenoid GDGT membrane lipids and their producers in the water column of a meromictic equatorial crater lake (Lake Chala, East Africa), Quaternary Science Reviews, 273, https://doi.org/10.1016/j.quascirev.2021.107263, 2021.

Bennike, O.: Palaeoecological studies of Holocene lake sediments from west Greenland, Palaeogeography, Palaeoclimatology, Palaeoecology, 155, 285–304, https://doi.org/10.1016/S0031-0182(99)00121-2, 2000.

Bennike, O., Anderson, N. J., and McGowan, S.: Holocene palaeoecology of southwest Greenland inferred from macrofossils in sediments of an oligosaline lake, J Paleolimnol, 43, 787–798, https://doi.org/10.1007/s10933-009-9368-x, 2010.

Besseling, M. A., Hopmans, E. C., Boschman, R. C., Sinninghe Damsté, J. S., and Villanueva, L.: Benthic archaea as potential sources of tetraether membrane lipids in sediments across an oxygen minimum zone, Biogeosciences, 15, 4047–4064, https://doi.org/10.5194/bg-15-4047-2018, 2018.

Bittner, L., De Jonge, C., Gil-Romera, G., Lamb, H. F., Russell, J. M., and Zech, M.: A Holocene temperature (brGDGT) record from Garba Guracha, a high-altitude lake in Ethiopia, Biogeosciences, 19, 5357–5374, https://doi.org/10.5194/bg-19-5357-2022, 2022.

Blaauw, M. and Christen, J. A.: Flexible Paleoclimate Age-Depth Models Using an Autoregressive Gamma Process, Bayesian Anal, 6, 457–474, https://doi.org/10.1214/ba/1339616472, 2011.

Blaga, C. I., Reichart, G.-J., Heiri, O., and Sinninghe Damsté, J. S.: Tetraether membrane lipid distributions in water-column particulate matter and sediments: a study of 47 European lakes along a north–south transect, Journal of Paleolimnology, 41, 523–540, https://doi.org/10.1007/s10933-008-9242-2, 2009.

Blaga, C. I., Reichart, G.-J., Vissers, E. W., Lotter, A. F., Anselmetti, F. S., and Sinninghe Damsté, J. S.: Seasonal changes in glycerol dialkyl glycerol tetraether concentrations and fluxes in a perialpine lake: Implications for the use of the TEX86 and BIT proxies, Geochimica et Cosmochimica Acta, 75, 6416–6428, https://doi.org/10.1016/j.gca.2011.08.016, 2011.

Box, J. E., Nielsen, K. P., Yang, X., Niwano, M., Wehrlé, A., van As, D., Fettweis, X., Køltzow, M. A. Ø., Palmason, B., Fausto, R. S., van den Broeke, M. R., Huai, B., Ahlstrøm, A. P., Langley, K., Dachauer, A., and Noël, B.: Greenland ice sheet rainfall climatology, extremes and atmospheric river rapids, Meteorological Applications, 30, e2134, https://doi.org/10.1002/met.2134, 2023.

van Bree, L. G. J., Peterse, F., Baxter, A. J., De Crop, W., van Grinsven, S., Villanueva, L., Verschuren, D., and Sinninghe Damsté, J. S.: Seasonal variability and sources of in situ brGDGT production in a permanently stratified African crater lake, Biogeosciences, 17, 5443–5463, https://doi.org/10.5194/bg-17-5443-2020, 2020.

Briner, J. P., Kaufman, D. S., Bennike, O., and Kosnik, M. A.: Amino acid ratios in reworked marine bivalve shells constrain Greenland Ice Sheet history during the Holocene, Geology, 42, 75–78, https://doi.org/10.1130/G34843.1, 2014.

Briner, J. P., McKay, N. P., Axford, Y., Bennike, O., Bradley, R. S., De Vernal, A., Fisher, D., Francus, P., Fréchette, B., Gajewski, K., Jennings, A., Kaufman, D. S., Miller, G., Rouston, C., and Wagner, B.: Holocene climate change in Arctic Canada and Greenland, Quaternary Science Reviews, 147, 340–364, https://doi.org/10.1016/j.quascirev.2016.02.010, 2016.

Briner, J. P., Cuzzone, J. K., Badgeley, J. A., Young, N. E., Steig, E. J., Morlighem, M., Schlegel, N.-J., Hakim, G. J., Schaefer, J. M., Johnson, J. V., Lesnek, A. J., Thomas, E. K., Allan, E., Bennike, O., Cluett, A. A., Csatho, B., De Vernal, A., Downs, J., Larour, E., and Nowicki, S.: Rate of mass loss from the Greenland Ice Sheet will exceed Holocene values this century, Nature, 586, 70–74, https://doi.org/10.1038/s41586-020-2742-6, 2020.

Buckles, L. K., Villanueva, L., Weijers, J. W., Verschuren, D., and Damste, J. S.: Linking isoprenoidal GDGT membrane lipid distributions with gene abundances of ammonia-oxidizing Thaumarchaeota and uncultured crenarchaeotal groups in the water column of a tropical lake (Lake Challa, East Africa), Environmental Microbiology, 15, 2445–62, https://doi.org/10.1111/1462-2920.12118, 2013.

Buckles, L. K., Weijers, J. W. H., Verschuren, D., and Sinninghe Damsté, J. S.: Sources of core and intact branched tetraether membrane lipids in the lacustrine environment: Anatomy of Lake Challa and its catchment, equatorial East Africa, Geochimica et Cosmochimica Acta, 140, 106–126, https://doi.org/10.1016/j.gca.2014.04.042, 2014.

Butler, T. M., Wilhelm, A.-C., Dwyer, A. C., Webb, P. N., Baldwin, A. L., and Techtmann, S. M.: Microbial Community Dynamics During Lake Ice Freezing, Sci Rep, 9, 6231, https://doi.org/10.1038/s41598-019-42609-9, 2019.

Castañeda, I. S. and Schouten, S.: A review of molecular organic proxies for examining modern and ancient lacustrine environments, Quaternary Science Reviews, 30, 2851–2891, https://doi.org/10.1016/j.quascirev.2011.07.009, 2011.

Cluett, A. A., Thomas, E. K., Evans, S. M., and Keys, P. W.: Seasonal Variations in Moisture Origin Explain Spatial Contrast in Precipitation Isotope Seasonality on Coastal Western Greenland, JGR Atmospheres, 126, e2020JD033543, https://doi.org/10.1029/2020JD033543, 2021.

Cluett, A. A., Thomas, E. K., McKay, N. P., Cowling, O. C., Castañeda, I. S., and Morrill, C.: Lake Dynamics Modulate the Air Temperature Variability Recorded by Sedimentary Aquatic Biomarkers: A Holocene Case Study From Western Greenland, JGR Biogeosciences, 128, e2022JG007106, https://doi.org/10.1029/2022JG007106, 2023.

Colcord, D. E., Cadieux, S. B., Brassell, S. C., Castañeda, I. S., Pratt, L. M., and White, J. R.: Assessment of branched GDGTs as temperature proxies in sedimentary records from several small lakes in southwestern Greenland, Organic Geochemistry, 82, 33–41, https://doi.org/10.1016/j.orggeochem.2015.02.005, 2015.

Corcoran, M. C., Thomas, E. K., and Morrill, C.: Using a Paired Chironomid $\delta^{18}O$ and Aquatic Leaf Wax $\delta^{2}H$ Approach to Reconstruct Seasonality on Western Greenland During the Holocene, Paleoceanog and Paleoclimatol, 36, e2020PA004169, https://doi.org/10.1029/2020PA004169, 2021.

Cronauer, S. L., Briner, J. P., Kelley, S. E., Zimmerman, S. R. H., and Morlighem, M.: 10Be dating reveals early-middle Holocene age of the Drygalski Moraines in central West Greenland, Quaternary Science Reviews, 147, 59–68, https://doi.org/10.1016/j.quascirev.2015.08.034, 2016.

Dang, X., Ding, W., Yang, H., Pancost, R. D., Naafs, B. D. A., Xue, J., Lin, X., Lu, J., and Xie, S.: Different temperature dependence of the bacterial brGDGT isomers in 35 Chinese lake sediments compared to that in soils, Organic Geochemistry, 119, 72–79, https://doi.org/10.1016/j.orggeochem.2018.02.008, 2018.

De Jonge, C., Stadnitskaia, A., Hopmans, E. C., Cherkashov, G., Fedotov, A., and Sinninghe Damsté, J. S.: In situ produced branched glycerol dialkyl glycerol tetraethers in suspended particulate matter from the Yenisei River, Eastern Siberia, Geochimica et Cosmochimica Acta, 125, 476–491, https://doi.org/10.1016/j.gca.2013.10.031, 2014.

Dee, S. G., Russell, J. M., Morrill, C., Chen, Z., and Neary, A.: PRYSM v2.0: A Proxy System Model for Lacustrine Archives, Paleoceanog and Paleoclimatol, 33, 1250–1269, https://doi.org/10.1029/2018PA003413, 2018.

Downs, J., Johnson, J., Briner, J., Young, N., Lesnek, A., and Cuzzone, J.: Western Greenland ice sheet retreat history reveals elevated precipitation during the Holocene thermal maximum, The Cryosphere, 14, 1121–1137, https://doi.org/10.5194/tc-14-1121-2020, 2020.

Dufour, A., Zolina, O., and Gulev, S. K.: Atmospheric Moisture Transport to the Arctic: Assessment of Reanalyses and Analysis of Transport Components, Journal of Climate, 29, 5061–5081, https://doi.org/10.1175/JCLI-D-15-0559.1, 2016.

Dutton, A., Carlson, A. E., Long, A. J., Milne, G. A., Clark, P. U., DeConto, R., Horton, B. P., Rahmstorf, S., and Raymo, M. E.: Sea-level rise due to polar ice-sheet mass loss during past warm periods, Science, 349, aaa4019, https://doi.org/10.1126/science.aaa4019, 2015.

Eggermont, H. and Heiri, O.: The chironomid-temperature relationship: expression in nature and palaeoenvironmental implications, Biological Reviews, 87, 430–456, https://doi.org/10.1111/j.1469-185X.2011.00206.x, 2012.

England, M. R., Eisenman, I., Lutsko, N. J., and Wagner, T. J. W.: The Recent Emergence of Arctic Amplification, Geophysical Research Letters, 48, e2021GL094086, https://doi.org/10.1029/2021GL094086, 2021.

Feng, X., Zhao, C., D'Andrea, W. J., Liang, J., Zhou, A., and Shen, J.: Temperature fluctuations during the Common Era in subtropical southwestern China inferred from brGDGTs in a remote alpine lake, Earth and Planetary Science Letters, 510, 26–36, https://doi.org/10.1016/j.epsl.2018.12.028, 2019.

*Fisher, M., *Stafford, T., Moon, T., and Thurber, A.: QGreenland, , https://doi.org/10.5281/zenodo.8326507, 2023.

Frechette, B. and de Vernal, A.: Relationship between Holocene climate variations over southern Greenland and eastern Baffin Island and synoptic circulation pattern, Clim. Past, 2009.

Frederikse, T., Landerer, F., Caron, L., Adhikari, S., Parkes, D., Humphrey, V. W., Dangendorf, S., Hogarth, P., Zanna, L., Cheng, L., and Wu, Y.-H.: The causes of sea-level rise since 1900, Nature, 584, 393–397, https://doi.org/10.1038/s41586-020-2591-3, 2020.

Fredskild, B.: Studies in the Vegetational History of Greenland, Palaeobotanical Investigations of some Holocene Lake and Bog deposits., Meddr Grønland, 198, https://doi.org/10.7146/mog.v198.147748, 1973.

Fredskild, B.: The Holocene vegetational development of the Godthåbsfjord area, West Greenland, Meddelelser om Grønland. Geoscience, 10, 28 pp.-28 pp., https://doi.org/10.7146/moggeosci.v10i.140322, 1983.

Gajewski, K.: Quantitative reconstruction of Holocene temperatures across the Canadian Arctic and Greenland, Global and Planetary Change, 128, 14–23, https://doi.org/10.1016/j.gloplacha.2015.02.003, 2015.

Gibb, O. T., Steinhauer, S., Fréchette, B., de Vernal, A., and Hillaire-Marcel, C.: Diachronous evolution of sea surface conditions in the Labrador Sea and Baffin Bay since the last deglaciation, The Holocene, 25, 1882–1897, https://doi.org/10.1177/0959683615591352, 2015.

Hansen, K. E., Giraudeau, J., Wacker, L., Pearce, C., and Seidenkrantz, M.-S.: Reconstruction of Holocene oceanographic conditions in eastern Baffin Bay, Climate of the Past, 16, 1075–1095, https://doi.org/10.5194/cp-16-1075-2020, 2020.

Hopmans, E. C., Schouten, S., and Sinninghe Damsté, J. S.: The effect of improved chromatography on GDGT-based palaeoproxies, Organic Geochemistry, 93, 1–6, https://doi.org/10.1016/j.orggeochem.2015.12.006, 2016.

Hostetler, S. W. and Bartlein, P. J.: Simulation of lake evaporation with application to modeling lake level variations of Harney-Malheur Lake, Oregon, Water Resources Research, 26, 2603–2612, https://doi.org/10.1029/WR026i010p02603, 1990.

IPCC: AR6 Climate Change 2021: The Physical Science Basis, Intergovernmental pannel on climate change, Geneva, 2021.

Jane, S. F., Mincer, J. L., Lau, M. P., Lewis, A. S. L., Stetler, J. T., and Rose, K. C.: Longer duration of seasonal stratification contributes to widespread increases in lake hypoxia and anoxia, Global Change Biology, 29, 1009–1023, https://doi.org/10.1111/gcb.16525, 2023.

Kaplan, M. R., Wolfe, A. P., and Miller, G. H.: Holocene Environmental Variability in Southern Greenland Inferred from Lake Sediments, Quat. res., 58, 149–159, https://doi.org/10.1006/qres.2002.2352, 2002.

Karami, M., Hansen, B. U., Westergaard-Nielsen, A., Abermann, J., Lund, M., Schmidt, N. M., and Elberling, B.: Vegetation phenology gradients along the west and east coasts of Greenland from 2001 to 2015, Ambio, 46, 94–105, https://doi.org/10.1007/s13280-016-0866-6, 2017.

Kaufman, D.: Holocene thermal maximum in the western Arctic (0–180°W), Quaternary Science Reviews, 23, 529–560, https://doi.org/10.1016/j.quascirev.2003.09.007, 2004.

Kaufman, D., McKay, N., Routson, C., Erb, M., Dätwyler, C., Sommer, P. S., Heiri, O., and Davis, B.: Holocene global mean surface temperature, a multi-method reconstruction approach, Sci Data, 7, 201, https://doi.org/10.1038/s41597-020-0530-7, 2020.

Kerimoglu, O. and Rinke, K.: Stratification dynamics in a shallow reservoir under different hydro-meteorological scenarios and operational strategies, Water Resources Research, 49, 7518–7527, https://doi.org/10.1002/2013WR013520, 2013.

Kettle, H., Thompson, R., Anderson, N. J., and Livingstone, D. M.: Empirical modeling of summer lake surface temperatures in southwest Greenland, Limnology and Oceanography, 49, 271–282, https://doi.org/10.4319/lo.2004.49.1.0271, 2004.

Klanten, Y., Couture, R. -M., Christoffersen, K. S., Vincent, W. F., and Antoniades, D.: Oxygen Depletion in Arctic Lakes: Circumpolar Trends, Biogeochemical Processes, and Implications of Climate Change, Global Biogeochemical Cycles, 37, e2022GB007616, https://doi.org/10.1029/2022GB007616, 2023.

Klanten, Y., MacIntyre, S., Fitzpatrick, C., Vincent, W. F., and Antoniades, D.: Regime Shifts in Lake Oxygen and Temperature in the Rapidly Warming High Arctic, Geophysical Research Letters, 51, e2023GL106985, https://doi.org/10.1029/2023GL106985, 2024.

Kobashi, T., Menviel, L., Jeltsch-Thömmes, A., Vinther, B. M., Box, J. E., Muscheler, R., Nakaegawa, T., Pfister, P. L., Döring, M., Leuenberger, M., Wanner, H., and Ohmura, A.: Volcanic influence on centennial to millennial Holocene Greenland temperature change, Sci Rep, 7, 1441, https://doi.org/10.1038/s41598-017-01451-7, 2017.

Larocca, L. J. and Axford, Y.: Arctic glaciers and ice caps through the Holocene:a circumpolar synthesis of lake-based reconstructions, Climate of the Past, 18, 579–606, https://doi.org/10.5194/cp-18-579-2022, 2022.

Larocca, L. J., Axford, Y., Bjørk, A. A., Lasher, G. E., and Brooks, J. P.: Local glaciers record delayed peak Holocene warmth in south Greenland, Quaternary Science Reviews, 241, 106421, https://doi.org/10.1016/j.quascirev.2020.106421, 2020.

Larsen, N. K., Kjær, K. H., Lecavalier, B., Bjørk, A. A., Colding, S., Huybrechts, P., Jakobsen, K. E., Kjeldsen, K. K., Knudsen, K.-L., Odgaard, B. V., and Olsen, J.: The response of the southern Greenland ice sheet to the Holocene thermal maximum, Geology, 43, 291–294, https://doi.org/10.1130/G36476.1, 2015.

Larsen, N. K., Strunk, A., Levy, L. B., Olsen, J., Bjørk, A., Lauridsen, T. L., Jeppesen, E., and Davidson, T. A.: Strong altitudinal control on the response of local glaciers to Holocene climate change in southwest Greenland, Quaternary Science Reviews, 168, 69–78, https://doi.org/10.1016/j.quascirev.2017.05.008, 2017.

Lasher, G. E., Axford, Y., Masterson, A. L., Berman, K., and Larocca, L. J.: Holocene temperature and landscape history of southwest Greenland inferred from isotope and geochemical lake sediment proxies, Quaternary Science Reviews, 239, 106358, https://doi.org/10.1016/j.quascirev.2020.106358, 2020.

Laskar, J., Robutel, P., Joutel, F., Gastineau, M., Correia, A. C. M., and Levrard, B.: A long-term numerical solution for the insolation quantities of the Earth, A&A, 428, 261–285, https://doi.org/10.1051/0004-6361:20041335, 2004.

Lazier, J., Hendry, R., Clarke, A., Yashayaev, I., and Rhines, P.: Convection and restratification in the Labrador Sea, 1990–2000, Deep Sea Research Part I: Oceanographic Research Papers, 49, 1819–1835, https://doi.org/10.1016/S0967-0637(02)00064-X, 2002.

Leger, T. P. M., Clark, C. D., Huynh, C., Jones, S., Ely, J. C., Bradley, S. L., Diemont, C., and Hughes, A. L. C.: A Greenland-wide empirical reconstruction of paleo ice sheet retreat informed by ice extent markers: PaleoGrIS version 1.0, Clim. Past, 20, 701–755, https://doi.org/10.5194/cp-20-701-2024, 2024.

Lesnek, A. J., Briner, J. P., Young, N. E., and Cuzzone, J. K.: Maximum Southwest Greenland Ice Sheet Recession in the Early Holocene, Geophysical Research Letters, 47, e2019GL083164, https://doi.org/10.1029/2019GL083164, 2020.

Liang, J., Chevalier, M., Liu, K., Perfumo, A., Wang, M., Xie, H., Hou, J., Herzschuh, U., and Chen, F.: Discrepancies in lacustrine bacterial lipid temperature reconstructions explained by microbial ecology, Commun Earth Environ, 5, 1–14, https://doi.org/10.1038/s43247-024-01925-3, 2024.

Lindberg, K. R., Daniels, W. C., Castañeda, I. S., and Brigham-Grette, J.: Biomarker proxy records of Arctic climate change during the Mid-Pleistocene transition from Lake El'gygytgyn (Far East Russia), Clim. Past, 18, 559–577, https://doi.org/10.5194/cp-18-559-2022, 2022.

Lindborg, T., Rydberg, J., Tröjbom, M., Berglund, S., Johansson, E., Löfgren, A., Saetre, P., Nordén, S., Sohlenius, G., Andersson, E., Petrone, J., Borgiel, M., Kautsky, U., and Laudon, H.: Biogeochemical data from terrestrial and aquatic ecosystems in a periglacial catchment, West Greenland, Earth System Science Data, 8, 439–459, https://doi.org/10.5194/essd-8-439-2016, 2016.

Liu, Z., Zhu, J., Rosenthal, Y., Zhang, X., Otto-Bliesner, B. L., Timmermann, A., Smith, R. S., Lohmann, G., Zheng, W., and Elison Timm, O.: The Holocene temperature conundrum, Proceedings of the National Academy of Sciences, 111, E3501-5, https://doi.org/10.1073/pnas.1407229111, 2014.

Loomis, S. E., Russell, J. M., Eggermont, H., Verschuren, D., and Sinninghe Damsté, J. S.: Effects of temperature, pH and nutrient concentration on branched GDGT distributions in East African lakes: Implications for paleoenvironmental reconstruction, Organic Geochemistry, 66, 25–37, https://doi.org/10.1016/j.orggeochem.2013.10.012, 2014a.

Loomis, S. E., Russell, J. M., Heureux, A. M., D'Andrea, W. J., and Sinninghe Damsté, J. S.: Seasonal variability of branched glycerol dialkyl glycerol tetraethers (brGDGTs) in a temperate lake system, Geochimica et Cosmochimica Acta, 144, 173–187, https://doi.org/10.1016/j.gca.2014.08.027, 2014b.

MacIntyre, S., Cortés, A., and Sadro, S.: Sediment respiration drives circulation and production of CO_2 in ice-covered Alaskan arctic lakes, Limnol Oceanogr Letters, 3, 302–310, https://doi.org/10.1002/lol2.10083, 2018.

Martin, C., Ménot, G., Thouveny, N., Peyron, O., Andrieu-Ponel, V., Montade, V., Davtian, N., Reille, M., and Bard, E.: Early Holocene Thermal Maximum recorded by branched tetraethers and pollen in Western Europe (Massif Central, France), Quaternary Science Reviews, 228, https://doi.org/10.1016/j.quascirev.2019.106109, 2020.

Martin, K. C., Buizert, C., Brook, E., Williams, O. L., Edwards, J. S., Riddell-Young, B., Fudge, T. J., Mederbel, F., Beaudette, R., Severinghaus, J., Oyabu, I., Kawamura, K., Kirk, M., Koldtoft, I., Steffensen, J. P., and Blunier, T.: Greenland Ice Cores Reveal a South-To-North Difference in Holocene Thermal Maximum Timings, Geophysical Research Letters, 51, e2024GL111405, https://doi.org/10.1029/2024GL111405, 2024.

Martínez-Sosa, P., Tierney, J. E., Stefanescu, I. C., Dearing Crampton-Flood, E., Shuman, B. N., and Routson, C.: A global Bayesian temperature calibration for lacustrine brGDGTs, Geochimica et Cosmochimica Acta, 305, 87–105, https://doi.org/10.1016/j.gca.2021.04.038, 2021.

Massé, S., Botrel, M., Walsh, D. A., and Maranger, R.: Annual nitrification dynamics in a seasonally ice-covered lake, PLOS ONE, 14, e0213748, https://doi.org/10.1371/journal.pone.0213748, 2019.

Masson-Delmotte, V., Landais, A., Stievenard, M., Cattani, O., Falourd, S., Jouzel, J., Johnsen, S. J., Dahl-Jensen, D., Sveinsbjornsdottir, A., White, J. W. C., Popp, T., and Fischer, H.: Holocene climatic changes in Greenland: Different deuterium excess signals at Greenland Ice Core Project (GRIP) and NorthGRIP, Journal of Geophysical Research: Atmospheres, 110, https://doi.org/10.1029/2004JD005575, 2005.

McFarlin, J. M., Axford, Y., Kusch, S., Masterson, A. L., Lasher, G. E., and Osburn, M. R.: Aquatic plant wax hydrogen and carbon isotopes in Greenland lakes record shifts in methane cycling during past Holocene warming, Sci. Adv., 9, eadh9704, https://doi.org/10.1126/sciadv.adh9704, 2023.

McKay, N. P., Emile-Geay, J., and Khider, D.: geoChronR – an R package to model, analyze, and visualize age-uncertain data, Geochronology, 3, 149–169, https://doi.org/10.5194/gchron-3-149-2021, 2021.

Miller, D. R., Habicht, M. H., Keisling, B. A., Castañeda, I. S., and Bradley, R. S.: A 900-year New England temperature reconstruction from in situ seasonally produced branched glycerol dialkyl glycerol tetraethers (brGDGTs), Climate of Past, 2018.

Moon, T., Fisher, M., Stafford, T., and Harden, L.: QGreenland (3.0.0), https://doi.org/10.5281/zenodo.12823307, 2023.

Morrill, C., Meador, E., Livneh, B., Liefert, D. T., and Shuman, B. N.: Quantitative model-data comparison of mid-Holocene lake-level change in the central Rocky Mountains, Climate Dynamics, 53, 1077–1094, https://doi.org/10.1007/s00382-019-04633-3, 2019.

Muñoz Sabater, J.: ERA5-Land hourly data from 1950 to present. Copernicus Climate Change Service (C3S) Climate Data Store (CDS), https://doi.org/10.24381/cds.e2161bac, 2019.

Novak, J. B., Russell, J. M., Lindemuth, E. R., Prokopenko, A. A., Pérez-Angel, L., Zhao, B., Swann, G. E. A., and Polissar, P. J.: The Branched GDGT Isomer Ratio Refines Lacustrine Paleotemperature Estimates, Geochem Geophys Geosyst, 26, e2024GC012069, https://doi.org/10.1029/2024GC012069, 2025.

Nusbaumer, J., Alexander, P. M., LeGrande, A. N., and Tedesco, M.: Spatial Shift of Greenland Moisture Sources Related to Enhanced Arctic Warming, Geophysical Research Letters, 46, 14723–14731, https://doi.org/10.1029/2019GL084633, 2019.

Otiniano, G., Thomas, Elizabeth. K., Castañeda, I. S., Acharya, S., and Mark, S.: chromatoPy, 2025.

Otiniano, G. A., Porter, T. J., Buceta, R. E., Bergman, M. E., and Phillips, M. A.: Climatic and environmentally driven variability in lacustrine brGDGT distributions at local to regional scales in Alaska and northwestern Canada, Organic Geochemistry, 181, https://doi.org/10.1016/j.orggeochem.2023.104604, 2023.

Otiniano, G. A., Porter, T. J., Phillips, M. A., Juutinen, S., Weckström, J. B., and Heikkilä, M. P.: Reconstructing warm-season temperatures using brGDGTs and assessing biases in Holocene temperature records in northern Fennoscandia, Quaternary Science Reviews, 329, 108555, https://doi.org/10.1016/j.quascirev.2024.108555, 2024.

Ouellet-Bernier, M.-M., De Vernal, A., Hillaire-Marcel, C., and Moros, M.: Paleoceanographic changes in the Disko Bugt area, West Greenland, during the Holocene, The Holocene, 24, 1573–1583, https://doi.org/10.1177/0959683614544060, 2014.

Pepin, N., Bradley, R. S., Diaz, H. F., Baraer, M., Caceres, E. B., Forsythe, N., Fowler, H., Greenwood, G., Hashmi, M. Z., Liu, X. D., Miller, J. R., Ning, L., Ohmura, A., Palazzi, E., Rangwala, I., Schöner, W., Severskiy, I., Shahgedanova, M., Wang, M. B., Williamson, S. N., Yang, D. Q., and Mountain Research Initiative EDW Working Group: Elevation-dependent warming in mountain regions of the world, Nature Clim Change, 5, 424–430, https://doi.org/10.1038/nclimate2563, 2015.

Perner, K., Moros, M., Jennings, A., Lloyd, J., and Knudsen, K.: Holocene palaeoceanographic evolution off West Greenland, The Holocene, 23, 374–387, https://doi.org/10.1177/0959683612460785, 2013.

Piccolroaz, S., Woolway, R. I., and Merchant, C. J.: Global reconstruction of twentieth century lake surface water temperature reveals different warming trends depending on the climatic zone, Climatic Change, 160, 427–442, https://doi.org/10.1007/s10584-020-02663-z, 2020.

Porter, C., Howat, I., Noh, M.-J., Husby, E., Khuvis, S., Danish, E., Tomko, K., Gardiner, J., Negrete, A., Yadav, B., Klassen, J., Kelleher, C., Cloutier, M., Bakker, J., Enos, J., Arnold, G., Bauer, G., and Morin, P.: ArcticDEM - Strips, Version 4.1 (V1), https://doi.org/10.7910/DVN/C98DVS, 2022.

Prowse, T., Alfredsen, K., Beltaos, S., Bonsal, B., Duguay, C., Korhola, A., McNamara, J., Pienitz, R., Vincent, W. F., Vuglinsky, V., and Weyhenmeyer, G. A.: Past and Future Changes in Arctic Lake and River Ice, AMBIO, 40, 53–62, https://doi.org/10.1007/s13280-011-0216-7, 2011.

Raberg, J. H., Harning, D. J., Crump, S. E., de Wet, G., Blumm, A., Kopf, S., Geirsdóttir, Á., Miller, G. H., and Sepúlveda, J.: Revised fractional abundances and warm-season temperatures substantially improve brGDGT calibrations in lake sediments, Biogeosciences, 18, 3579–3603, https://doi.org/10.5194/bg-18-3579-2021, 2021.

Raberg, J. H., Miller, G. H., Geirsdóttir, Á., and Sepúlveda, J.: Near-universal trends in brGDGT lipid distributions in nature, Science advances, 8, eabm7625, https://doi.org/10.1126/sciadv.abm7625, 2022.

Raberg, J. H., de Wet, G. A., Geirsdóttir, Á., Sepúlveda, J., and Miller, G. H.: Oxygen Depletion in Lake Waters May Skew brGDGT-Inferred Temperatures by More Than 10°C, Geophysical Research Letters, 52, e2024GL113562, https://doi.org/10.1029/2024GL113562, 2025.

Rantanen, M., Karpechko, A. Yu., Lipponen, A., Nordling, K., Hyvärinen, O., Ruosteenoja, K., Vihma, T., and Laaksonen, A.: The Arctic has warmed nearly four times faster than the globe since 1979, Commun Earth Environ, 3, 168, https://doi.org/10.1038/s43247-022-00498-3, 2022.

Reyes, F. R. and Lougheed, V. L.: Rapid Nutrient Release from Permafrost Thaw in Arctic Aquatic Ecosystems, Arctic, Antarctic, and Alpine Research, 47, 35–48, https://doi.org/10.1657/AAAR0013-099, 2015.

Russell, J. M., Hopmans, E. C., Loomis, S. E., Liang, J., and Sinninghe Damsté, J. S.: Distributions of 5- and 6-methyl branched glycerol dialkyl glycerol tetraethers (brGDGTs) in East African lake sediment: Effects of temperature, pH, and new lacustrine paleotemperature calibrations, Organic Geochemistry, 117, 56–69, https://doi.org/10.1016/j.orggeochem.2017.12.003, 2018.

Saini, J., Stein, R., Fahl, K., Weiser, J., Hebbeln, D., and Madaj, L.: Holocene variability in sea-ice conditions in the eastern Baffin Bay-Labrador Sea – A north–south biomarker transect study, Boreas, 51, 553–572, https://doi.org/10.1111/bor.12583, 2022.

Saros, J. E., Northington, R. M., Osburn, C. L., Burpee, B. T., and John Anderson, N.: Thermal stratification in small arctic lakes of southwest Greenland affected by water transparency and epilimnetic temperatures, Limnology and Oceanography, 61, 1530–1542, https://doi.org/10.1002/lno.10314, 2016.

Schneider, T., Castañeda, I. S., Zhao, B., Krüger, S., Salacup, J. M., and Bradley, R. S.: Tracing Holocene temperatures and human impact in a Greenlandic Lake: Novel insights from hyperspectral imaging and lipid biomarkers, Quaternary Science Reviews, 339, 108851, https://doi.org/10.1016/j.quascirev.2024.108851, 2024.

Schouten, S., Hopmans, E. C., Schefuß, E., and Damste, J. S. S.: Distributional variations in marine crenarchaeotal membrane lipids: a new tool for reconstructing ancient sea water temperatures?, Earth and Planetary Science Letters, 204, 265–274, 2002.

Schouten, S., Hopmans, E. C., and Damste, J. S. S.: The organic geochemistry of glycerol dialkyl glycerol tetraether lipids: A review, Organic Geochemistry, 54, 19–61, https://doi.org/10.1016/j.orggeochem.2012.09.006, 2013.

Schweinsberg, A. D., Briner, J. P., Miller, G. H., Bennike, O., and Thomas, E. K.: Local glaciation in West Greenland linked to North Atlantic Ocean circulation during the Holocene, Geology, 45, 195–198, https://doi.org/10.1130/G38114.1, 2017.

Schweinsberg, A. D., Briner, J. P., Licciardi, J. M., Bennike, O., Lifton, N. A., Graham, B. L., Young, N. E., Schaefer, J. M., and Zimmerman, S. H.: Multiple independent records of local glacier variability on Nuussuaq, West Greenland, during the Holocene, Quaternary Science Reviews, 215, 253–271, https://doi.org/10.1016/j.quascirev.2019.05.007, 2019.

Seneviratne, S. I. and Hauser, M.: Regional Climate Sensitivity of Climate Extremes in CMIP6 Versus CMIP5 Multimodel Ensembles, Earth's Future, 8, e2019EF001474, https://doi.org/10.1029/2019EF001474, 2020.

Shanahan, T. M., Hughen, K. A., and Van Mooy, B. A. S.: Temperature sensitivity of branched and isoprenoid GDGTs in Arctic lakes, Organic Geochemistry, 64, 119–128, https://doi.org/10.1016/j.orggeochem.2013.09.010, 2013.

Sinninghe Damsté, J. S., Hopmans, E. C., Pancost, R. D., Schouten, S., and Geenevasen, J. A.: Newly discovered non-isoprenoid glycerol dialkyl glycerol tetraether lipids in sediments, Chemical Communications, 1683–1684, 2000.

Sinninghe Damsté, J. S., Ossebaar, J., Abbas, B., Schouten, S., and Verschuren, D.: Fluxes and distribution of tetraether lipids in an equatorial African lake: Constraints on the application of the TEX86 palaeothermometer and BIT index in lacustrine settings, Geochimica et Cosmochimica Acta, 73, 4232–4249, https://doi.org/10.1016/j.gca.2009.04.022, 2009.

Sweeney, A. J., Fu, Q., Po-Chedley, S., Wang, H., and Wang, M.: Internal Variability Increased Arctic Amplification During 1980–2022, Geophysical Research Letters, 50, e2023GL106060, https://doi.org/10.1029/2023GL106060, 2023.

Thoman, R. L., Moon, T. A., and Druckenmiller, M. L.: NOAA Arctic Report Card 2023 : Executive Summary, https://doi.org/10.25923/5VFA-K694, 2023.

Thomas, E. K., Briner, J. P., Ryan-Henry, J. J., and Huang, Y.: A major increase in winter snowfall during the middle Holocene on western Greenland caused by reduced sea ice in Baffin Bay and the Labrador Sea, Geophysical Research Letters, 43, 5302–5308, https://doi.org/10.1002/2016GL068513, 2016.

Thomas, E. K., Castañeda, I. S., McKay, N. P., Briner, J. P., Salacup, J. M., Nguyen, K. Q., and Schweinsberg, A. D.: A Wetter Arctic Coincident With Hemispheric Warming 8,000 Years Ago, Geophysical Research Letters, 45, https://doi.org/10.1029/2018GL079517, 2018.

Thomas, E. K., Cluett, A. A., Erb, M. P., McKay, N. P., Briner, J. P., Castañeda, I. S., Corcoran, M. C., Cowling, O. C., Gorbey, D. B., Lindberg, K. R., Prince, K. K., and Salacup, J.: Early Holocene Laurentide Ice Sheet Retreat Influenced Summer Atmospheric Circulation in Baffin Bay, Geophysical Research Letters, 50, https://doi.org/10.1029/2023gl103428, 2023.

Tierney, J. E., Schouten, S., Pitcher, A., Hopmans, E. C., and Sinninghe Damsté, J. S.: Core and intact polar glycerol dialkyl glycerol tetraethers (GDGTs) in Sand Pond, Warwick, Rhode Island (USA): Insights into the origin of lacustrine GDGTs, Geochimica et Cosmochimica Acta, 77, 561–581, https://doi.org/10.1016/j.gca.2011.10.018, 2012.

Vihma, T., Screen, J., Tjernström, M., Newton, B., Zhang, X., Popova, V., Deser, C., Holland, M., and Prowse, T.: The atmospheric role in the Arctic water cycle: A review on processes, past and future changes, and their impacts, Journal of Geophysical Research: Biogeosciences, 121, 586–620, https://doi.org/10.1002/2015JG003132, 2016.

Weber, Y., De Jonge, C., Rijpstra, W. I. C., Hopmans, E. C., Stadnitskaia, A., Schubert, C. J., Lehmann, M. F., Sinninghe Damsté, J. S., and Niemann, H.: Identification and carbon isotope composition of a novel branched GDGT isomer in lake sediments: Evidence for lacustrine branched GDGT production, Geochimica et Cosmochimica Acta, 154, 118–129, https://doi.org/10.1016/j.gca.2015.01.032, 2015.

Weber, Y., Sinninghe Damste, J. S., Zopfi, J., De Jonge, C., Gilli, A., Schubert, C. J., Lepori, F., Lehmann, M. F., and Niemann, H.: Redox-dependent niche differentiation provides evidence for multiple bacterial sources of glycerol tetraether lipids in lakes, Proceedings of the National Academy of Sciences, 115, 10926–10931, https://doi.org/10.1073/pnas.1805186115, 2018.

Westergaard-Nielsen, A., Hansen, B. U., Elberling, B., and Abermann, J.: Greenland Climates, in: Encyclopedia of the World's Biomes, edited by: Goldstein, M. I. and DellaSala, D. A., Elsevier, Oxford, 539–550, https://doi.org/10.1016/B978-0-12-409548-9.11750-6, 2020.

Wrona, F. J., Johansson, M., Culp, J. M., Jenkins, A., Mård, J., Myers-Smith, I. H., Prowse, T. D., Vincent, W. F., and Wookey, P. A.: Transitions in Arctic ecosystems: Ecological implications of a changing hydrological regime, Journal of Geophysical Research: Biogeosciences, 121, 650–674, https://doi.org/10.1002/2015JG003133, 2016.

Wu, J., Yang, H., Pancost, R. D., Naafs, B. D. A., Qian, S., Dang, X., Sun, H., Pei, H., Wang, R., Zhao, S., and Xie, S.: Variations in dissolved O2 in a Chinese lake drive changes in microbial communities and impact sedimentary GDGT distributions, Chemical Geology, 579, https://doi.org/10.1016/j.chemgeo.2021.120348, 2021.

Yang, Q., Dixon, T. H., Myers, P. G., Bonin, J., Chambers, D., van den Broeke, M. R., Ribergaard, M. H., and Mortensen, J.: Recent increases in Arctic freshwater flux affects Labrador Sea convection and Atlantic overturning circulation, Nat Commun, 7, 10525, https://doi.org/10.1038/ncomms10525, 2016.

Yao, Y., Zhao, J., Vachula, R. S., Werne, J. P., Wu, J., Song, X., and Huang, Y.: Correlation between the ratio of 5-methyl hexamethylated to pentamethylated branched GDGTs (HP5) and water depth reflects redox variations in stratified lakes, Organic Geochemistry, 147, https://doi.org/10.1016/j.orggeochem.2020.104076, 2020.

Young, N. E., Briner, J. P., Rood, D. H., Finkel, R. C., Corbett, L. B., and Bierman, P. R.: Age of the Fjord Stade moraines in the Disko Bugt region, western Greenland, and the 9.3 and 8.2 ka cooling events, Quaternary Science Reviews, 60, 76–90, https://doi.org/10.1016/j.quascirev.2012.09.028, 2013.

Young, N. E., Briner, J. P., Miller, G. H., Lesnek, A. J., Crump, S. E., Thomas, E. K., Pendleton, S. L., Cuzzone, J., Lamp, J., Zimmerman, S., Caffee, M., and Schaefer, J. M.: Deglaciation of the Greenland and Laurentide ice sheets interrupted by glacier advance during abrupt coolings, Quaternary Science Reviews, 229, 106091, https://doi.org/10.1016/j.quascirev.2019.106091, 2020.

Zhao, B., Castañeda, I. S., Bradley, R. S., Salacup, J. M., De Wet, G. A., Daniels, W. C., and Schneider, T.: Development of an in situ branched GDGT calibration in Lake 578, southern Greenland, Organic Geochemistry, 152, 104168, https://doi.org/10.1016/j.orggeochem.2020.104168, 2021.

Zhao, B., Russell, J. M., Tsai, V. C., Blaus, A., Parish, M. C., Liang, J., Wilk, A., Du, X., and Bush, M. B.: Evaluating global temperature calibrations for lacustrine branched GDGTs: Seasonal variability, paleoclimate implications, and future directions, Quaternary Science Reviews, 310, 108124, https://doi.org/10.1016/j.quascirev.2023.108124, 2023.